SCHOOL OF ADVANCED STUDIES OF THE ROMANIAN ACADEMY

DOCTORAL SCHOOL OF CHEMICAL SCIENCES

"PETRU PONI" INSTITUTE OF MACROMOLECULAR CHEMISTRY

CHEMISTRY Field

SYNTHESIS AND CHARACTERIZATION OF PHOTOREACTIVE POLYSACCHARIDE NETWORKS

SUMMARY OF DOCTORAL THESIS

PhD Supervisor:

CS I Dr. Sergiu COȘERI

PhD Student:

Ioana-Sabina TRIFAN

2025

ROMANIAN ACADEMY

"Petru Poni" Institute of Macromolecular Chemistry, Iași

We inform you that on October 31, 2025, at 10:00, in the Conference Hall of the "Petru Poni" Institute of Macromolecular Chemistry in Iaşi, the public defense of the doctoral thesis entitled "Synthesis and characterization of photoreactive polysaccharide networks", author Ioana-Sabina Trifan, will take place, to achieve the scientific title of doctor.

PRESIDENT: ***CS I Dr. Habil. Valeria Harabagiu***
"Petru Poni" Institute of Macromolecular Chemistry

SCIENTIFIC SUPERVISOR: ***CS I Dr. Habil. Sergiu Coșeri***
"Petru Poni" Institute of Macromolecular Chemistry, Iaşi

COMMITTEE MEMBERS: ***CS II Dr. Diana-Elena Ciolacu***
"Petru Poni" Institute of Macromolecular Chemistry, Iaşi

Prof. Dr. Rodica-Mihaela Dinică
"Dunărea de Jos" University, Galați

Prof. Dr. Costel Moldoveanu
"Alexandru Ioan Cuza" University, Iași

In accordance with the Regulation on the organization and conduct of the doctoral program for the award of scientific titles in the Romanian Academy, we are sending you the summary of the doctoral thesis with the request to communicate your appreciations and observations. On this occasion, we invite you to participate in the public defense of the doctoral thesis.

Acknowledgements

With respect and sincerity, I would like to express my gratitude to my scientific supervisor, ***Dr. Sergiu Coșeri****, for the trust and indulgence given, for all the help provided during the doctoral internship, both for the development of a consistent thesis and for the training to become a skilled, hardworking and knowledge-hungry researcher. In addition to the proven perseverance, despite the fact that research is a meticulous work, with possible obstacles, your jovial character and note of optimism inspired me to overcome certain limits. Thank you and I appreciate you for the researcher and leader that you are!*

*Special thanks to the members of the supervision committee during the doctoral internship****,*** ***Dr. Violeta Melinte****,* ***Dr. Gabriela Biliuță*** *and* ***Dr. Daniela Ivanov*** *for their moral support and the numerous information intended to train me professionally.*

I would like to express my sincere thanks to the members of the doctoral committee, ***Dr. Diana-Elena Ciolacu****,* ***Prof. Dr. Rodica-Mihaela Dinică*** *and* ***Prof. Dr. Costel Moldoveanu****, for evaluating the content of the doctoral thesis and the suggestions offered, demonstrating kindness and availability.*

With great gratitude, I would like to thank all my colleagues, old and new, in the Department of ***"Polyaddition and Photochemistry"*** *for everything they have taught and advised me, both professionally and personally. I also thank you for the welcoming atmosphere in which I carry out my research activity!*

I thank my colleagues from other departments, with whom I have either had the pleasure of collaborating, sharing knowledge, or discussing various topics, for their advice and help, contributing to the development of the doctoral thesis or creating a conducive working environment.

Thanks to the ***"Petru Poni" Institute of Macromolecular Chemistry*** *and the* ***Romanian Academy*** *for the adequate environment dedicated to professional training and for the financial support provided during the doctoral internship.*

Full of emotions, I want to thank ***my mother and grandparents*** *for their unconditional and boundless love, for all their encouragement, but also for the necessary reprimands. You have built*

me up beautifully and I am grateful to you! I feel loved with you! You will always be my joy and peace, my source of motivation and "charging my batteries"!

I also want to express my gratitude to the ***Totolici and Manolescu families*** *who support me and are involved in my life to make me feel better. You are very dear to me!*

I am deeply grateful to ***my dear friends and colleagues*** *for their loyalty, determination in supporting me constantly and for many years, as well as for the sincerity with which they rejoice in my successes. You are wonderful!*

I would like to thank my friend, ***Narcis****, for the trust, support and patience he gives me! With you, everything seems easier to solve and more beautiful!*

Thank you!

Ioana-Sabina Trifan

My thoughts go not only to my loved ones, but also to the silent souls who watched over my steps with silent love, and to God, the unseen source of strength, hope, and inspiration who guided my path.

CONTENT

INTRODUCTION

The biopolymers type of macromolecular compounds continue to be studied with interest due to the benefits offered by their remarkable properties, among which the lack of toxicity and their immense structural variety and availability in nature, biocompatibility, are noteworthy. Polysaccharides represent a class of biopolymers with the greatest dynamic in research and exploitation due to their remarkable potential for implementation in many applications. It is worth noting that the use of natural polymers in the daily life of people, namely polysaccharides, has been documented since ancient times, long before their structure, formulas and compositions were discovered. As an example, native cellulose represents a material of great importance and use in the daily activities of people, regardless of the source from which it comes (wood, cotton, algae, etc.), as evidenced by the manufacture of papyrus - used as a material for notes by ancient Egyptians. The modification of the polysaccharide structures, through the chemical reactions in which they are involved, determines the emergence of new structures, implicitly new compounds - functional derivatives.

Current research in the field of polymer chemistry, carried out in laboratories around the world, aims not only to obtain and characterize new monomers and, implicitly, to create new types of polymers, but especially to identify and exploit polymers already reported in the scientific literature in new applications that would satisfy the increasingly high technological needs of various industries. As suggested by the name of this doctoral thesis – '**Synthesis and characterization of photoreactive polysaccharide networks**' – the **main purpose** of the study and the elaboration of the doctoral thesis, within the department of '**Polyaddition and Photochemistry**', aimed at obtaining and exploiting new polymers based on polysaccharides by introducing specific structural sequences, capable of giving them photochemical character. In this way, there is a considerable increase in the field of applicability in which polysaccharides and their derivatives could be used. Among the most common applications of polymers with photochemical properties are those related to the treatment of wastewaters, the pollutants being represented by industrial dyes and medicinal substances, or to the

manufacture of various medical devices. Taking into account these emerging fields, the polymeric materials developed and investigated in this thesis were tested for such applications.

The introductory part of the doctoral thesis presents in detail information about polysaccharide compounds, with an emphasis on those polysaccharides that were used in the experimental work, but also their main chemical reactions, reactions that lead the synthesis of new photoreactive polymers with diverse applications. The emphasis is placed mainly on the "key" aspects governing the field of photoreactive polymers: the study and understanding of the structural characteristics that confer photochemical properties, the evaluation and exploitation of the properties acquired by the final materials. The **theoretical part** is divided into four chapters; the first chapter highlights the importance of polysaccharides and functional derivatives in the context of the contemporary world, by presenting the structure, morphology, conformation and properties of the two polysaccharides extensively studied in this thesis: cellulose and pullulan. The functional derivatives of these two polysaccharides are not neglected either. After these sections, a large part is dedicated to the main chemical reactions in which cellulose and pullulan are involved, as well as the way in which these reactions influence their physicochemical properties. The second chapter is devoted to photoreactive polysaccharide networks. Photoreactive hydrogels of chemically modified polysaccharides are mainly discussed, attempting to classify these hydrogels according to the introduced components and photocatalytic properties. At the end of the second chapter, the importance of photochemical reactions through which hydrogels and polymer composites based on polysaccharides with photopolymerizable sequences are obtained is commented on, reviewing the initiators and photoinitiators used in such processes, as well as the mechanism of the radical photopolymerization reaction. The third chapter refers to the applications of hydrogels and composite materials based on chemically modified polysaccharides, with emphasis on those priority applications: the use of photoreactive composite materials for the treatment of contaminated waters, the use of injectable multi-crosslinked polysaccharide hydrogels in the administration and controlled release of drugs, but also the development of metal ion chemosensors through fluorescence studies. In the last chapter of the introductory part, the main conclusions about the topic addressed in the doctoral thesis are presented.

The second part of the doctoral thesis includes elements of originality, comprising the experimental data accumulated during the thesis preparation stage, which were processed,

analyzed, discussed, forming the basis of the scientific works published in the doctoral thesis portfolio. In an attempt to crystallize the main research directions that were addressed during the doctoral thesis, I could highlight the following:

- Synthesis of photopolymerizable cellulose acetate derivatives in the form of photocrosslinked films and investigation of the properties of these films
- Synthesis of materials with photocatalytic properties based on cellulose acetate and evaluation of their capacity to decompose organic dyes
- Synthesis of photopolymerizable cellulose derivatives, injectable hydrogels and study of their characteristic properties
- Synthesis of functional pullulan derivatives with fluorescent character acting as chemosensors for metal ions

The **first two directions** make up a consistent chapter of the doctoral thesis in which the necessary steps for the design of nanocomposites that serve as photochemical catalysts for the decomposition of organic dyes are described. A first step was to carry out reactions between cellulose acetate and an isocyanic compound with photopolymerizable methacrylic groups in order to obtain derivatives with different degrees of functionalization. The latter, by irradiation, led to the formation of photocrosslinked polymer films with varying degrees of crosslinking. The films obtained did not come only from methacrylic acetate derivatives, they were also obtained by combining these derivatives with other macromolecular compounds with photopolymerizable groups and relatively small molecular masses before irradiation in order to achieve a more versatile composition of the composites. The photocatalytic character of the final composites was given by the introduction of metal oxides and noble metal nanoparticles (inorganic compounds known for their photocatalytic activity) into the polymer matrix. The photocatalytic activity of the nanocomposites was tested in the degradation of four organic dyes and their efficiency in the decomposition of brilliant green dye was proven. Additional tests, such as the decomposition of binary mixtures of dyes, were conducted to fully investigate the photocatalytic properties. **Another research direction** involved the synthesis of hydrogels, based on cellulose or hydroxypropylcellulose and modified gelatin, with injectable properties, which would have the potential for applicability in bone tissue healing. The use of these materials in medical applications can be explained by the photopolymerizable structural sequences introduced into the structure through cascade

chemical reactions: the oxidation of polysaccharides with different oxidizing agents (TEMPO radical and sodium periodate – $NaIO_4$ – for cellulose and sodium hypochlorite – NaClO – for its derivative), followed by reactions of these oxidized products, but also of gelatin with methacrylic anhydride. Also, studies conducted to investigate the degradation in solutions that mimic biological fluids, the liquid absorption capacity and the injectability properties have demonstrated that the hydrogels in question are feasible for such applications, but these experiments require complementary studies, which will be the subject of my future research. The use of pullulan in the preparation of polymers with photopolymerizable sequences was not accidental, this polysaccharide has a series of unique properties compared to other polysaccharides, such as: biocompatibility, biodegradability, ease of film formation, water solubility, lack of toxicity. The obtaining of the new polymeric derivatives, based on pullulan, was carried out in two stages: oxidation with different oxidizing agents (TEMPO radical or sodium periodate–$NaIO_4$) and coupling reactions between the newly formed groups (carboxylic, respectively carbonyl) from the oxidized derivatives and aromatic amines. The fluorescent character was easily highlighted in the case of the pullulan derivative with imine bonds and nitrile groups, for which the metal ion detection capacity was investigated using fluorescence studies and it was proven to have a strong affinity for trivalent iron (Fe^{3+}) and then copper (Cu^{2+}) ions. Such metal ions are found in polluted waters and predispose living organisms to serious diseases once ingested. Several tests were needed to confirm the ability of the fluorescent compound to capture metal ions, but consistent evidence is seen from the fluorescence spectra, when, by adding metal ions to the polymer solution, the intensity of the emission band is reduced. In addition to the directions discussed previously, the thesis also contains a subchapter dedicated to the synthesis and physico-chemical characterization of injectable, multi-crosslinked (physical and chemical crosslinking) hydrogels based on pullulan and polyvinyl alcohol (PVA). In this experiment, hydrogels were obtained by performing reactions between PVA and previously oxidized pullulan using TEMPO or $NaIO_4$ (with ester crosslinks originating from carboxylic groups and/or hydrogen bonds) or PVA and coupling products between oxidized pullulan derivatives and a boronic acid derivative (hydrogen bonds, ester bonds originating from carboxylic groups or boronic acid, and amide or imine bonds). Through this study, I wanted to expose the advantages for which these hydrogels can be used in a similar way to the composites developed in the first two research directions, being able to

be support matrices for metallic nanoparticles. Future studies refer to the introduction of photosensitive sequences to form other type of crosslinks, in addition to the existing ones – photochemical crosslinks.

The studies that make up the content of the thesis deal with several aspects, from different branches of chemistry (macromolecular and organic through the reactions carried out, inorganic through the preparation of solutions of inorganic compounds and the manipulation of salts, coordinative through the investigation of chemical complexes, analytical through the analysis techniques), which are intertwined to a certain extent with other exact sciences (biology, mathematics). Among the conclusions that can be drawn from the studies discussed in the doctoral thesis, the role of compounds with photochemical properties in various applications, which are different, depending on the functional groups and structural sequences introduced into the starting polysaccharides (methacrylic, imine, nitrile, ketone groups, benzene nuclei), is highlighted. The doctoral thesis contains 220 pages, 155 figures, 25 tables, 14 mathematical formulas and 136 references.

PART II – SELF CONTRIBUTIONS
DESIGN, SYNTHESIS AND CHARACTERIZATION OF PHOTORESPONSIVE NETWORKS WITH POLYSACCHARIDE COMPONENTS

1. POLYSACCHARIDES USED FOR THE DESIGN OF PHOTORESPONSIVE MATERIALS

Some polysaccharide derivatives are recognized by their gelation capacity, forming hydrogels or organogels, while other types of derivatives are used to obtain photocrosslinked polymer networks, each finding its appropriate applications, according to the properties it possesses. Thus, it is very important that when planning and designing a new material, the physical and rheological properties of the polysaccharides or their derivatives that will be used in the production of that material are decisively taken into account, as these properties decisively dictate the final properties of the product [87]. In the experimental part, which presents my own contribution, the polysaccharides used were cellulose, two of its derivatives - cellulose acetate and hydroxypropylcellulose - and pullulan. The main reasons why these polysaccharides were used in the present study are the structural differences between cellulose and pullulan, the increased solubility of pullulan in water compared to that of other

polysaccharides, implicitly cellulose (insoluble in this solvent) and the fact that cellulose is the most widespread biopolymer, but also the common properties such as: regenerability, biocompatibility and biodegradability.

2. POLYSACCHARIDIC MATERIALS WITH PHOTOCHEMICAL ACTIVITY

2.1. Photocrosslinked nanocomposites based on cellulose acetate, cerium oxide and noble metals

2.1.1. Design of nanocomposites

This subchapter describes the synthesis of hybrid composites by creating heterojunctions between organic and inorganic compounds chosen as components. To form the organic component of the composites, cellulose diacetate was chosen instead of cellulose, as it has an increased solubility compared to cellulose in organic solvents [87]. Thus, the **first experiment** (**Figure 1**) consisted in carrying out a series of chemical reactions between cellulose acetate (CA) solubilized in THF and 2-isocyanatoethyl methacrylate (2-IEMA), in the presence of dibutyltin dilaurate (DD) catalyst which led to the formation of CA functional derivatives with methcrylate groups grafted *via* urethane linkages and degree of functionalization of 5% (CA-M5), 10% (CA-M10), 25% (CA-M25), 50% (CA-M50) and 100% (CA-M100) [88]. The importance of grafting these pendant groups was due to the fact that they are photosensitive, and the addition of the photoinitiator Irgacure 819 and irradiation with a UV light source allowed crosslinking, as well as the synthesis of materials with increased strength and durability, which could serve as matrices for the inclusion of photocatalyst nanoparticles. In order to obtain crosslinkable films under the action of UV light, the photobehavior of cellulose derivatives functionalized with methacrylic units was studied by FTIR spectroscopy. The degree of conversion (CD(%)) of the double bond was evaluated by monitoring the intensity of the absorption bands characteristic of the methacrylic double bond that undergo important spectral changes during UV irradiation. Since the values obtained for CD(%) were moderate, it was decided to increase the degree of crosslinking of the derivatives by using a second macromolecular compound, used as a comonomer–the urethane-methacrylic derivative of castor oil (CO-UDMA) or the urethane-methacrylic derivative of polypropylene glycol (PPG-M) [87,89]. According to studies, CO-UDMA proved to have increased photoreactivity, making it a perfect candidate to be used in combination with the CA-M10 derivative, resulting

in an organic matrix with flexibility and transparency suitable for the targeted application. The **second experiment** consisted of the synthesis of hybrid nanocomposites, using CA-M10 and CO-UDMA derivatives, CeO_2 nanoparticles and noble metal nanoparticles, CeO_2 being chosen due to the electronic configuration of Ce^{4+} on the valence layer ($[Xe]4f^{1}5d^{1}$) which facilitates the transfer of electrons from adsorbed organic molecules to oxygen species [90]. The other inorganic component of the composites is represented by Au, Ag and Pd nanoparticles synthesized by photochemical route simultaneously with the formation of the organic matrix because it favors the photocatalytic activity of the composite material. The reaction consists of the reduction of nanoparticles from the corresponding metal salts of $AuBr_3$, $AgNO_3$ and $Pd(NO_3)_2 \times 2H_2O$ [91]. **Figure 2** schematically represents the transformations during the photopolymerization of polymers: the formation of crosslinks, their type and the generation of noble metal nanoparticles.

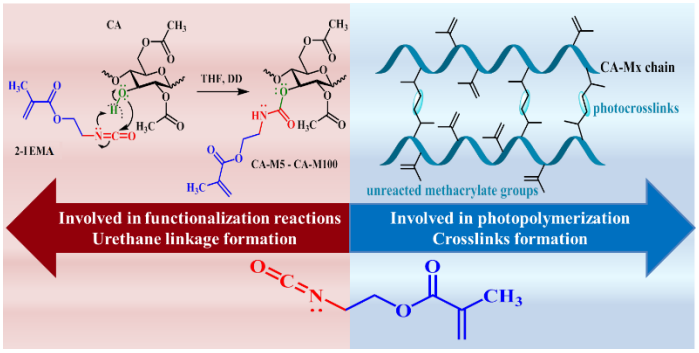

Figure 1. Representation of the methacrylate CA derivatives preparation, as well as the formation of the corresponding photocrosslinked networks.

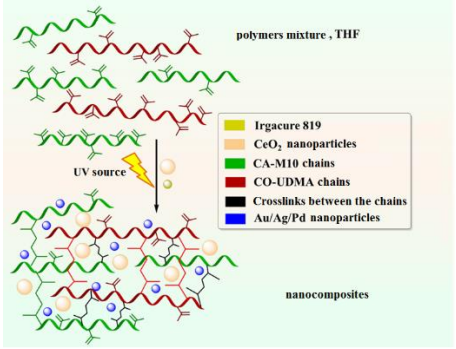

Figure 2. Synthesis of composites based on CA-M10, CO-UDMA, CeO_2 nanoparticles and Au, Ag or Pd.

Table 1. Gravimetric ratios (%) of the components of the photoreactive composites.

			Percentage of the total quantity used (wt%)					
			CA-MA	CO-UDMA	CeO_2	$AgNO_3$	$AuBr_3$	$Pd(NO_3)_2 \times 2H_2O$
Series I	1	F1	50	50	-	-	-	-
	2	F1-Ce	50	50	5	-	-	-
	3	F1-CeAg	50	50	5	1	-	-
	4	F1-CeAu	50	50	5	-	1	-
	5	F1-CePd	50	50	5	-	-	1
Series II	1	F2	70	30	-	-	-	-
	2	F2-Ce	70	30	5	-	-	-
	3	F2-CeAg	70	30	5	1	-	-
	4	F2-CeAu	70	30	5	-	1	-
	5	F2-CePd	70	30	5	-	-	1

2.1.2. Physico-chemical characterization of urethane-methacrylic derivatives and hybrid nanocomposites

2.1.2.1. Physico-chemical characterization of urethane-methacrylic derivatives

The transmittance FTIR spectrum of the CA compound shows absorption bands due to the O-H vibrations of the hydroxyl groups at 3447 cm^{-1} and bands attributed to the vibrations of the C=O bond of the ester group at 1744 cm^{-1}. Unlike the spectrum of the CA compound, in which there are no absorption bands at 815 cm^{-1} or 1638 cm^{-1}, the spectra of the synthesized derivatives show these two bands characteristic of the C=C double bonds of the methacrylic groups grafted onto the CA polymer chains, denoting the success of the functionalization. The ^{1}H-NMR spectra illustrate the peaks for CA, but also the peaks of the functional derivatives that are attributed to the protons of the methacrylic sequences grafted onto the polymer chains. Thus, in the CA spectrum, the signals of the peaks characteristic of the anhydroglucose units appear in the aliphatic region (3.4-4 ppm).

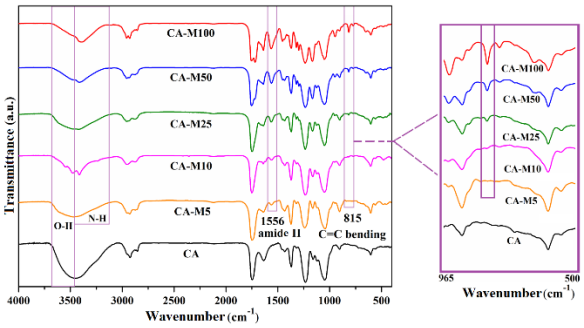

Figure 3. FTIR transmittance spectra for CA and CA derivatives (CA-M5–CA-M100).

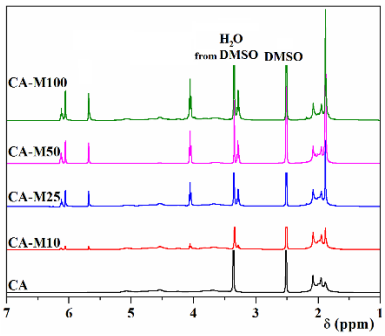

Figure 4. ^{1}H-RMN spectra of CA and CA derivatives (CA-M5–CA-M100).

The spectra of the functional derivatives show signals at 1.9 ppm corresponding to methyl protons attached to double bonds, at 3.4 and 3.7 ppm, being assigned to methylene protons attached to urethane bonds, and at 5.6 and 6.1 ppm, respectively, the signals being given by protons belonging to C=C double bonds appear [57]. In addition to identifying chemical structures and confirming the success of the grafting reaction, this spectral technique also has the advantage of calculating the degree of functionalization experimentally and comparing it with the theoretical one, through the ratio of the number of unsaturated protons (3.6-4 ppm) and the number of protons in the repeating units (4.3-5.2 ppm). Other analyses performed to investigate the CA derivatives were XRD analysis, which provided information about the semi-crystalline regions of the compounds (attributed to the elongated peak at 8.6°

for CA and all derivatives except CA-M100, in which spectrum it is absent) and crystalline regions (associated with the peaks at 13°, 17° and, especially, at 21.5°, which suggest an improvement in the organization of the polymer chains through the functionalization reactions performed), SEM analysis, and morphology studies indicating compact, homogeneous regions with few small pores. Following measurements to determine the water contact angle, the behavior of each compound proved to be hydrophilic due to angle values below 90º. The average value of the angle formed by CA with the water droplet was 62 ± 1º. The change in contact angles indicates the success of the functionalization of the CA compound.

2.1.2.2. Physico-chemical characterization of hybrid nanocomposites

The polymer films belonging to both types of series present in the ATR-FTIR spectra (**Figure 5**) O-H and N-H bands at 3400 cm^{-1}, characteristic of the hydroxyl and urethane groups present in the structure of the photopolymerizable derivatives. The success of the photopolymerization, implicitly the formation of the crosslinked networks, is marked by the decrease in intensity of the bands attributed to the photosensitive groups, found in the spectra at 813 cm^{-1} and 1638 cm^{-1} [58].

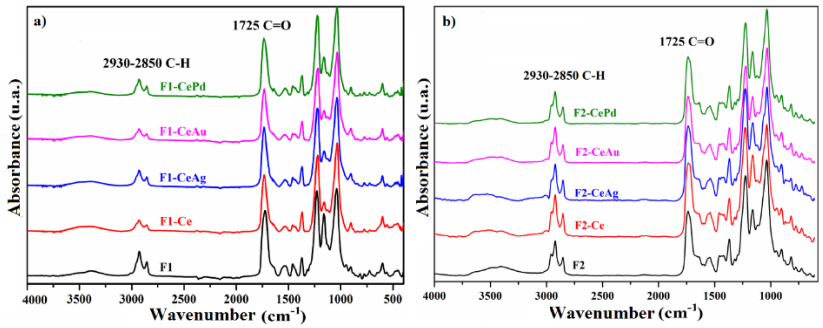

Figure 5. ATR-FTIR absorbance spectra of photopolymerized films based on CA-M10, CO-UDMA and/or CeO_2, Ag, Au, Pd nanoparticles – I series **(a)** and II series **(b)**.

In the diffractograms of polymer films from the II series, intense peaks are found, characteristic of semi-crystalline regions in the CA structure [96]. For composites with photogenerated nanoparticles, new peaks are distinguished at 38.3º (F2-CeAg), 44.7º and 64.9º (F2-CeAu) and 40.1º (F2-CePd). Although weak in intensity, the appearance of these peaks and their correlation with the (111) diffraction plane of CeO_2 nanocrystals, implicitly with the diffraction peak at 28.8º, demonstrate the *in situ* photochemical formation of metal nanoparticles from precursors. From the SEM images in the fracture, it is observed that in the polymer films without included nanoparticles, small variations in the composition of the samples (series I – 50% CA and 50% CO-UDMA, respectively series II – 70% CA and 30%

CO-UDMA) determine different organizations of the films in section. Thus, the pore size in the composition of the F1 film is small due to the small percentage of CA introduced, while the simple film of series II, with a high percentage of CA, presents large pores called macropores. These variations are caused by viscosity variations since CA-M10 is a white, solid compound, and CO-UDMA is a viscous fluid. During the photopolymerization reaction, which is a diffusion-controlled process, viscosity differences can influence the movement of polymer molecules and their reorganization. The photocrosslinking reaction rate of the F1 film is higher, compared to that of the F2 film, so that the sample presents a dense porous structure. In contrast, the F2 film presents a morphology with larger pores included in a more compact organization of the material. In the case of the films with included catalyst nanoparticles (F1-Ce and F2-Ce), the morphology is not affected by the inclusion of the inorganic component. Similarly, the films containing noble metal nanoparticles are not morphologically affected by the *in situ* photogeneration of the nanoparticles. By energy dispersive X-ray spectroscopy (EDX), the chemical elements found in the composition of the films with CeO_2 nanoparticles and those with CeO_2 and noble metal nanoparticles could be identified. From the TEM images, it was observed that the metal oxide nanoparticles are well dispersed in the polymer matrix. The sizes of CeO_2 nanoparticles ranged between 10-40 nm [97,98]. In their vicinity, smaller nanoparticles (5-15 nm), round in shape and prone to agglomeration – photogenerated metal nanoparticles – were identified. The thermal stability of the F1, F1-Ce and F1-CeAg films was analyzed. From the TG and DTG curves, it is observed that the films are stable for the photocatalytic applications for which they were prepared. The amount of residue for F1 at 700ºC was 13%, while, for the other samples analyzed, the residue was somewhat higher, namely 16.3% for the F1-Ce sample and ~21% for the F1-CeAg sample, demonstrating the presence of inorganic nanoparticles in the films by their contribution to the amount of residue.

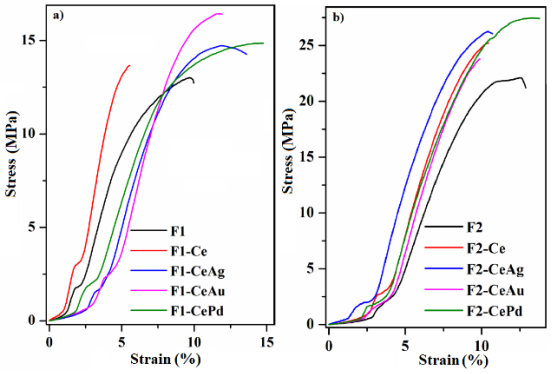

Figure 6. Stress-strain curves for polymer films of I series **(a)** and II series **(b)**.

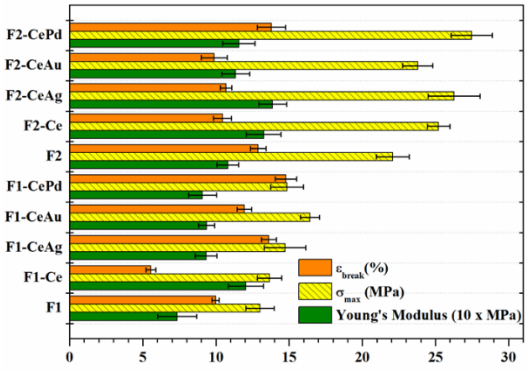

Figure 7. Parameters for determining the mechanical properties of films in I and II series.

The mechanical properties were investigated and it was found that the organic part of the composition influences especially σ_{max}, with higher values being observed for films in series II than for series I, which demonstrates that the functionalized CA offers higher mechanical strength compared to the castor oil derivative. The inclusion of CeO_2 nanoparticles in the films induced an improvement in the Young's modulus for F1-Ce and F2-Ce (**Figure 7**), while the photogeneration of noble metal nanoparticles seems to have induced a plasticizing effect in most of the composites. No major differences were recorded between the films in the same series, the materials being classified as materials with good mechanical properties. The incorporation of CeO_2, Ag, Au and Pd nanoparticles produced substantial changes in the optical properties of the simple polymer networks (F1 and F2) which are transparent to visible light and in the UV range up to 340 nm of the wavelength. Films containing only CeO_2 nanoparticles (F1-Ce and F2-Ce) as inorganic components have an intense yellow color, and the other films acquire different shades (brown–F1-CeAg, F2-CeAg, purple–F1-CeAu, F2-CeAu and black–F1-CePd, F2-CePd) as a result of the photogeneration of metallic nanoparticles. Photocatalytic materials are characterized by their band gap energy (E_g), the value of which can be modified by various chemical reactions and processes, leading in the case of reduction to improved catalytic activity. Studies have shown that CeO_2 nanoparticles exhibit an absorption maximum at λ = 308 nm, having a band gap value of Eg=3.02 eV, which confirms that they can be used as catalysts for photochemical reactions by UV light irradiation [97]. Their incorporation into the organic matrix produces an increase in light absorption up to wavelengths with almost 50-70 units higher (λ=360–380 nm). *In situ* photogeneration of metal nanoparticles from precursors enhances the catalytic character of the metal oxide already improved by its inclusion in support matrices. Photogeneration of Ag nanoparticles causes the formation of the absorption band at $\lambda_{max} \approx$ 434 nm, while Au nanoparticles contribute to the formation of the characteristic plasmon at $\lambda_{max} \approx$540 nm. The appearance of intense absorption bands in the spectra of the films containing Ag and Au correspons to localized surface plasmon resonance and is attributed to the type of spherical nanoparticles as seen in the SEM images. The films containing Pd nanoparticles do not show defined absorption bands in the visible region, but the absorption band edges and transmission band edges of F1-CePd and F2-CePd are shifted towards the red component of the visible range, indicating an increased absorption of photons.

2.1.3. Study of photopolymerization kinetics of urethane-methacrylic derivatives

2.1.3.1. Investigation of the urethane-methacrylic derivatives of cellulose acetate the photopolymerization kinetics

The evolution of the photopolymerization reactions of the CA-M5 – CA-M100 derivatives was monitored by FTIR spectroscopy. The FTIR spectra, measured as a function of the irradiation time, illustrate the decrease of the absorption bands at 815 cm^{-1} characteristic of the C=C double bonds. Based on the obtained conversion degrees, it can be deduced that during the photopolymerization, the CD(%) and the reaction rates were strongly influenced by the reduction of the distance between the functional groups. The maximum value of CD(%) after 300 seconds of irradiation, corresponding to the CA-M100 film, was 55.14%. The CD(%) values for each polymer film are presented in **Figure 9**. Considering that the values obtained for CD(%) are relatively moderate and that there were no major changes in the absorption band during irradiation, it was desired to optimize the method by combining the CA derivatives with compounds known for their photoreactivity.

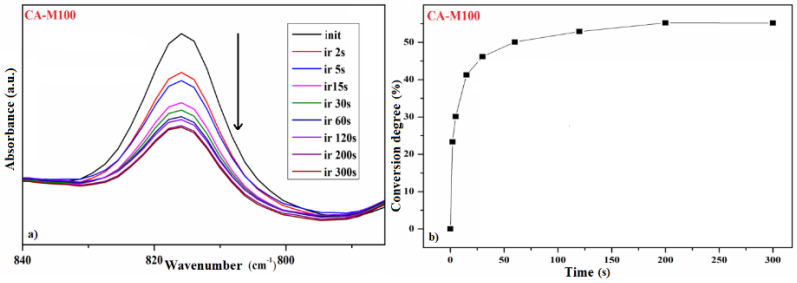

Figure 8. Monitoring of the band at 815 cm^{-1} during irradiation **(a)** and the curve of the conversion degree of photopolymerizable bonds as a function of time **(b)**.

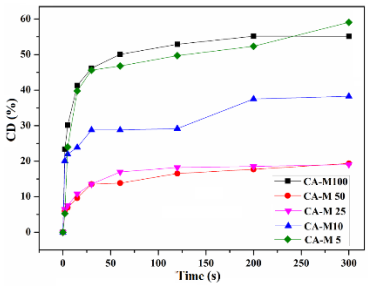

Figure 9. CD(%) curves of C=C bonds in derivatives as a function of irradiation time.

2.1.3.2. Investigation of the photopolymerization kinetics of urethane-methacrylic derivatives of cellulose acetate in mixture with photopolymerizable compounds

Polysaccharides have high molecular weights, diverse structures, as we have shown in the previous sections, and are susceptible to functionalization reactions with various (photo)reactive groups. A method for improving the crosslinking density of CA derivatives refers to the introduction of macromolecular compounds, with photosensitive sequences, with which, by combining, the CA derivatives form homogeneous mixtures. Among the promising compounds in this case, those with relatively low molecular weight are preferable due to the flexibility offered.

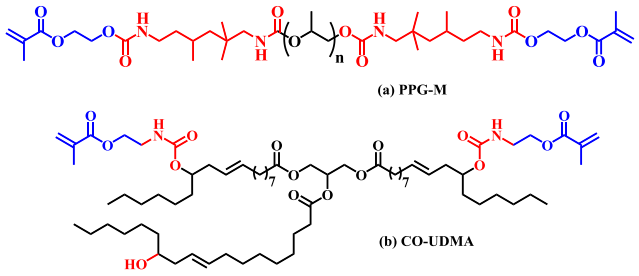

Figure 10. Chemical structures of PPG-M and CO-UDMA polymers used in combination with CA derivatives to improve the photopolymerization process.

Thus, CD(%) and crosslink density are increased by forming polymer films based on these combinations, the most appropriate explanation being related to the decrease in the distance between the photoreactive groups on the polymer chains. Considering the chemical structure, the relatively low molecular weight, as well as the ability to form transparent films, polypropylene glycol modified with urethane-methacrylic sequences (PPG-M) (**Figure 10a**) and castor oil derivative functionalized with the same type of sequences (CO-UDMA) (**Figure 10b**) were chosen as monomers in the formation of films based on CA derivatives. Initially, the FTIR absorbance spectra were recorded as a function of the irradiation time. The decrease in the intensity of the bands characteristic of methacrylic groups, from 815 cm^{-1}, was monitored by interpreting the spectra of films based on CA and PPG-M or CO-UDMA. The evolution of the photopolymerization reactions of the CA-M–CO-UDMA and CA-M–PPG-M polymer films was investigated, more precisely the absorption bands at 815 cm^{-1} at different irradiation times and the characteristic curves of the photopolymerization degrees of the films as a function of time. It was observed that the polymer film formed by CA-M100 and CO-UDMA presents higher values of the degree of crosslinking, the maximum value being 76%. The maximum value of the CD(%) for the CA-M10–CO-UDMA film was approximately 60%. For the CA-M–PPG-M series of films, the CD(%) obtained after 300 seconds of photoirradiation varied between 49%-70%. The conversion of photopolymerizable bonds in the CA-M10–PPG-M film reached a plateau after 200 seconds of irradiation, the value determined in the 300th second being 59%. It is observed that CD(%) are sometimes higher for the modified CA and PPG-M films, and sometimes for the other type of composite films, but it can be seen that the formation of crosslinks in the CO-UDMA-based films is significant (high CD(%)) from the beginning, in the first seconds of irradiation, unlike the PPG-M-based films where the important changes occur later during irradiation. According to the results, both compounds used as monomers contributed to improving the CD(%) of the photopolymerizable

sequences corresponding to each irradiation time and to improving the crosslinking degrees of the polymer networks.

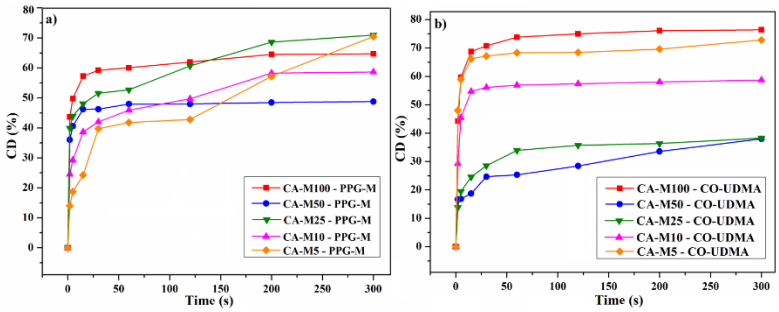

Figure 11. CD(%) curves of C=C bonds as a function of irradiation time in films of CA derivatives with PPG-M **(a)** and CO-UDMA **(b)**.

Unlike the rest of the polymer networks based on CA derivatives, the networks based on CA-M10 have similar CD(%) values (approximately 59%), regardless of whether they contain PPG-M or CO-UDMA as the second component. Following the analysis of the transparency and flexibility of the films and the results obtained from the double bond photoconversion kinetics, it was found that CO-UDMA is much more suitable to be combined with CA derivatives, especially CA-M10, with CeO_2 and Ag, Au or Pd nanoparticles to form nanocomposites with a medium degree of crosslinking to confer flexibility to the films.

2.1.4. Applications– photochemical decomposition of organic pollutants in wastewater

Although metal oxides have good photocatalytic activity, being often used to decompose organic waste in water, being composed of a single phase, they fail to absorb photons from the entire solar spectrum, which is why it was desired to improve their catalytic performance, more precisely, absorption in a wider range of electromagnetic radiation, this being possible by introducing them into polymer matrices (forming hybrid nanocomposites) [104]. The organic pollutants chosen to follow the photochemical decomposition in the presence of hybrid catalysts are: Congo red, brilliant green, rhodamine B and 4-nitrophenol. The solutions had the following molar concentrations: c = 5×10^{-6} M for the Congo red solution; c = 2×10^{-5} M for the brilliant green solution; c = 10^{-5} M for the rhodamine B solution; c = 10^{-4} M for the 4-nitrophenol solution. The time required for the brilliant green pollutant to be completely degraded varied depending on the nanocomposite film used as the photocatalyst. Based on the time-dependent monitoring of the maximum absorbance band at 624 nm in the UV-vis spectrum, it was demonstrated that of the polymer film series I, F1-CeAg was the most efficient, degrading the pollutant in only 60 minutes. According to the C_t/C_0 versus time plots

of polymer films series I and II and the $\ln(C_t/C_0)$ versus time plots of series I and II, the photocatalytic performance varies as follows: F1-Ce≤F1-CeAu<F1-CePd<F1-CeAg and F2-Ce<F2-CeAu<F2-CeAg≤F2-CePd. Series I films show a better photocatalytic activity than series II films, and this may be due to the porous structure that leads to a larger surface area of the inorganic nanoparticles and better accessibility of the active centers. Therefore, the brilliant green dye diffuses more easily into the pores of series I photocatalysts than series II. Among all the nanocomposite films, F1-CeAg has the best efficiency in the photochemical degradation of the pollutant, reaching a maximum of 100% after 60 minutes of irradiation with a visible light source ($k=38.67\times10^{-3}$ min^{-1}). The tests carried out later consisted of evaluating the efficiency with which other organic pollutants (rhodamine B, Congo red, 4-nitrophenol) are decomposed by irradiation with visible light in the presence of F1-CeAg, the results being compared with those obtained in the case of the brilliant green derivative. Thus, the F1-CeAg photocatalyst shows good activity in the decomposition of 4-nitrophenol which is completely mineralized in 150 minutes. The time required for Congo red to be almost completely degraded is 200 minutes, while the photodegradation of rhodamine B is partial even after 250 minutes of irradiation. The rate constants with which the degradation of each pollutant occurs were determined from the $\ln(C_0/C_t)$ graph as a function of time for the entire time interval in which the reaction took place. The rate constant corresponding to the photodegradation of 4-nitrophenol was calculated, in the range 0-150 minutes, as $k=34.52\times10^{-3}$ min^{-1}, and the rate constant for the degradation of brilliant green dye was calculated, in the range 0-60 minutes, as $k=44.18\times10^{-3}$ min^{-1}. Having more complex structures, the photodegradation of Congo red and rhodamine B dyes requires a much longer irradiation time, so that after 200 minutes, the pollutants were still not completely degraded. In order to compare the results obtained and establish the efficiency of F1-CeAg on each pollutant, the degree of degradation after 60 minutes was calculated: 100% (brilliant green) > 84.5% (4-nitrophenol)≫37.1% (Congo red)>26.9% (rhodamine B). Thus, it was proven that F1-CeAg is a photocatalyst with good performance for the degradation of 4-nitrophenol and brilliant green. In this experiment, the influence of environmental pH on the catalytic activity of the composites was tested.

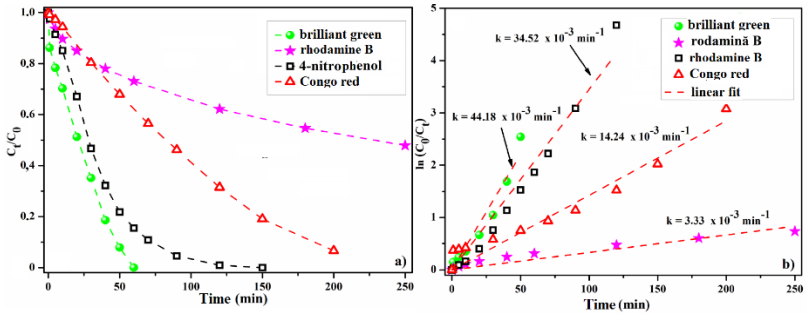

Figure 12. Time evolution of the photodegradation efficiency (C_0/C_t) of pollutants in the presence of F1-CeAg **(a)** and $\ln(C_0/C_t)$ as a function of time for photodegradation in the presence of F1-CeAg **(b)**.

The performance of the F1-CeAg film was investigated for the aqueous solution (pH=6.5) of brilliant green, but also for its buffer solutions (pH=4 and pH=9), all solutions being of concentration $c=2\times10^{-5}$ M. It was found that acidic and basic environments slightly inhibit the photodegradation of the dye. After 90 minutes of irradiation with a visible light source, in the presence of F1-CeAg, the percentage of dye degradation is ~95 % in both types of environments, with a process rate constant at pH=4 of $k=35.58\times10^{-3}$ min^{-1} and at pH=9 of $k=28.45\times10^{-3}$ min^{-1}. The optimal pH value for pollutant degradation in the presence of F1-CeAg is 6.5. As previously discussed, the F1-CeAg film was used for the photodecomposition of brilliant green dye both alone and in admixture with 4-nitrophenol, the process being carried out for five successive cycles. It was determined that the efficiency of the film decreases by about 4% after the completion of the five cycles of use, suggesting that the film is a suitable photocatalyst for such processes. For reuse, the F1-CeAg film was immersed in distilled water for 12 hours, dried and reused as a photocatalyst for the decomposition of brilliant green dye. It was found that the efficiency with which the dye is photochemically decomposed from its solution, after keeping it in a wet state (recycling) and drying, is 100%. The reuse of the F1-CeAg catalyst for the photodecomposition of BG was also investigated in acidic (pH = 4) and basic (pH = 9) media, and it was found that the catalytic efficiency has the same behavior as at pH = 6.5 and is reduced by only 6% after 5 cycles of use, indicating that the pH of the medium has no effect on the reuse of the F1-CeAg catalyst. Also, using FTIR spectroscopy and mass measurements, the integrity of the F1-CeAg film was also evaluated after its use in several photocatalytic cycles for the decomposition of the brilliant green solution. From the interpretation of the spectra, it was observed that there are no changes in the intensities of the absorption bands, therefore, the F1-CeAg film did not undergo structural

changes or mass losses (**Figure 14**). Considering all the results regarding the photocatalytic efficiency of the synthesized materials, it can be considered that the development of photocatalytic systems containing noble metal nanoparticles, in addition to catalyst nanoparticles and organic components acting as support matrices, increased the photocatalytic efficiency by changing the absorption of photons in the visible range.

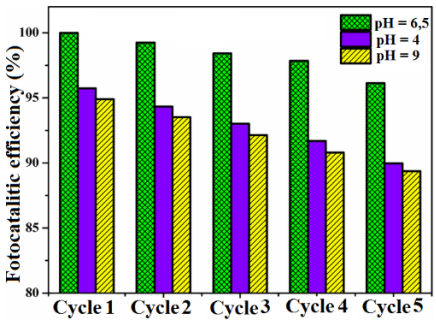

Figure 13. Reuse tests of F1-CeAg under visible light for its brilliant green degradation from aqueous solution and buffer solutions.

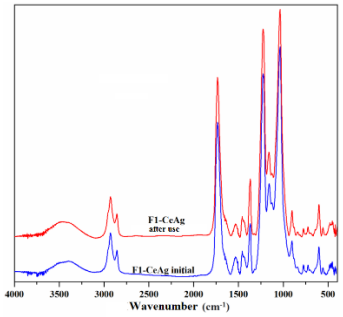

Figure 14. Reuse tests of F1-CeAg under visible light for its brilliant green degradation from aqueous solution and buffer solutions.

2.1.5. Conclusions

Hybrid composite photocatalyst systems are notable for the ease of recovery and reuse of materials compared to that of established photocatalysts, which is why the ability to eliminate some organic pollutants through photodegradation reactions and maintain catalytic efficiency upon reuse was discussed. The synthesis, characterization and evaluation of the photocatalytic properties of composites based on cellulose acetate modified with photopolymerizable sequences, castor oil modified with photosensitive groups, catalyst nanoparticles (CeO_2) and metal nanoparticles (Au, Ag, Pd) are the main aspects exposed in this chapter. As can be deduced from the SEM images, the combination of the two organic components must be achieved in an optimal gravimetric ratio in order to obtain good photocatalytic efficiency as in the case of film series I versus polymer film series II. The enhanced photocatalytic activity is also strongly observed in the case of nanocomposites synthesized photochemically concomitantly with the *in situ* photogeneration of metal nanoparticles. As an example, brilliant green was photodecomposed in the presence of F1-CeAg in half the time required for photodegradation in the presence of F1-Ce (120 minutes).

2.2. Injectable, photochemically crosslinked hydrogels based on cellulose and gelatin

2.2.1. Design of hydrogels

The hydrogels discussed in this subchapter were synthesized starting from polysaccharide compounds (cellulose or its water-soluble derivative – hydroxypropylcellulose (HPC)) and gelatin. The main characteristics targeted for these types of hydrogels were the induction of a photosensitivity to form photochemical crosslinks, injectability and their utilization in biomedical applications. The biopolymers were initially modified by selective oxidation reactions and methacrylates to graft photosensitive functions onto the polymer structure.

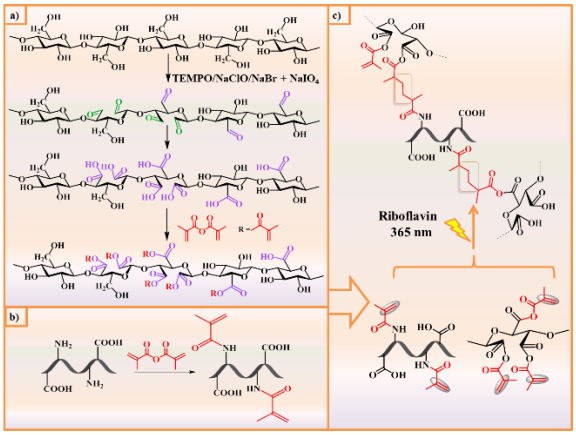

Figure 15. Representative scheme of the steps in the synthesis of CG hydrogel.

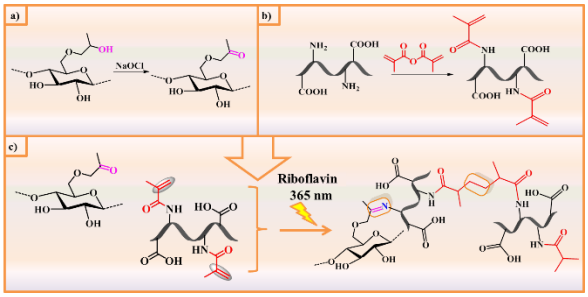

Figure 16. Representative scheme of the steps in the synthesis of HG hydrogel.

For the oxidation of cellulose, a well-established protocol was used, oxidation in the presence of TEMPO/NaClO/NaBr/$NaIO_4$. This oxidation system allows the simultaneous conversion of the three hydroxyl groups in the structural unit of cellulose into carboxyl groups [34]. The attachment of the photosensitive, methacrylic sequences was achieved following the reaction between the obtained carboxyl derivative (C-O) and methacrylic anhydride (C-O-MA). For the oxidation of HPC, NaClO was used, the secondary -OH groups of HPC being converted into ketone groups (formation of the oxidized derivative HPC-O). Similarly, sequences were grafted onto HPC-O, using methacrylic anhydride (formation of the derivative HPC-O-MA). Taking into account that gelatin cannot organize into ordered structures at the supramolecular level, it was decided to functionalize gelatin with methacrylic anhydride, thus facilitating the obtaining of three-dimensional structures. The reaction of gelatin with methacrylic anhydride occurs at the level of amine groups. In order to obtain different degrees

of methacrylation, different reaction times (2/4/6 or 8 hours) were used, the other parameters being kept constant – G-MA 2h, G-MA 4h, G-MA 6h and G-MA 8h. Starting from oxidized and methacrylated polysaccharide derivatives and methacrylated gelatin, in combination with a photoinitiator (riboflavin), physically and chemically double-crosslinked polymer networks were prepared (electrostatic interactions between the -COOH and -NH_2 groups and Schiff base bonds between -CHO and -NH_2, and then, under the action of UV radiation (λ= 365 nm), the formation of bridges between the methacrylate groups). In a similar way to the above hydrogels, hydrogels based on HPC-O-MA and G-MA were synthesized. The methacrylic derivative of gelatin in the composition of the photocrosslinked hydrogel (HG) obtained by irradiation under the same conditions as before was also G-MA 4h.

2.2.2. Characterization of compounds in the composition of hydrogels

The C-O and C-O-MA samples (**Figure 17**), in addition to the characteristic bands of the polysaccharide, also present a series of bands specific to oxidized and methacrylated compounds, thus confirming the success of the oxidation and methacrylation process. Thus, in the spectra of the functionalized derivatives a new band is found at 1600 cm^{-1}, attributed to the carboxylic groups (-COO-), this band being more pronounced in the spectrum of the oxidized compound than in that of the C-O-MA derivative, a sign that the oxidized groups have become ester groups with the C-O methacrylation reaction. In addition, in the spectrum of the C-O-MA compound, a band is identified at 1725 cm^{-1}, the band being specific both for *α,β*-unsaturated esters and for possible residues of unreacted conjugated anhydride. By comparative analysis of the NMR spectra (**Figure 18**), it was found that the methacrylation reaction of trioxidized cellulose (C-O) was successfully carried out, the clear proof being the appearance of proton signals characteristic of the groups in the methacrylic anhydride structure, in the areas 1-2.5 ppm and 5-6 ppm.

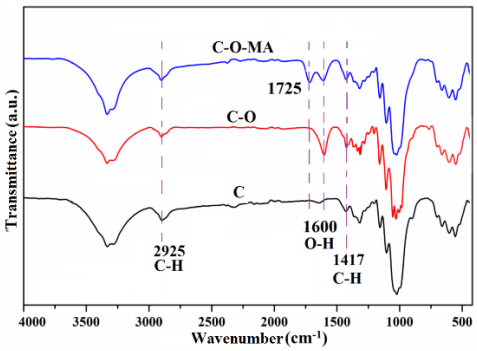

Figure 17. FTIR spectra of cellulose (C), C-O and C-O-MA.

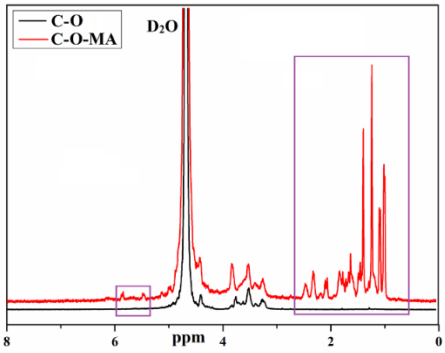

Figure 18. ^{1}H-RMN spectra of cellulose derivatives (C-O and C-O-MA).

Figure 19 shows the FTIR spectra of HPC and its derivatives. The oxidation of HPC, in the presence of NaClO, is evidenced by the band at 1620 cm^{-1}, characteristic of ketone groups. The band at 1725 cm^{-1}, assigned to newly formed ester groups, confirms the success of the methacrylation reaction of HPC-O, when the derivative HPC-O-MA is obtained.

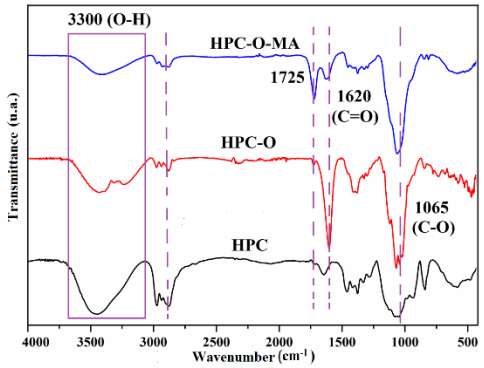

Figure 19. FTIR spectra of HPC, HPC-O and HPC-O-MA.

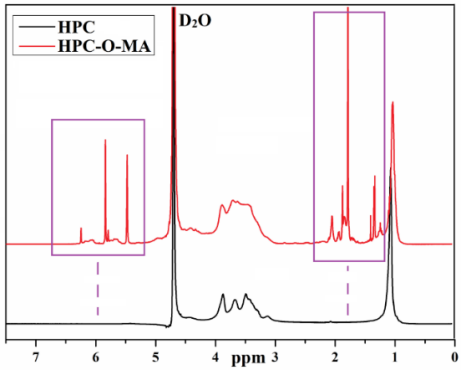

Figure 20. ^{1}H-RMN spectra of HPC and HPC-O-MA.

The bands at 3300 cm^{-1} (O-H) and 1065 cm^{-1} (C-O) undergo slight shifts or changes in intensity or a decrease in intensity, which confirms the synthesis of HPC derivatives. As in the case of C-O-MA, the success of grafting methacrylic anhydride sequences onto HPC-O chains was proven by proton spectra, where new signals were identified at 1-2.5 ppm and 5-6 ppm (from methacrylic groups). Through oxidation, the -OH groups of HPC were converted into ketone groups that cannot be identified in the proton spectra. Gelatin shows in the FTIR spectrum bands corresponding to amide groups at: 1638cm^{-1} (amide I), 1537cm^{-1} (amide II) and 1238 cm^{-1} (amide III). By reaction with methacrylic anhydride, the characteristic band of amide I increases in intensity, proving the success of the methacrylation. The success of the methacrylation of gelatin is proven in the NMR spectrum by the appearance of peaks at 5.4 and 5.7 ppm, attributed to the protons of the unsaturated groups grafted into the gelatin structure.

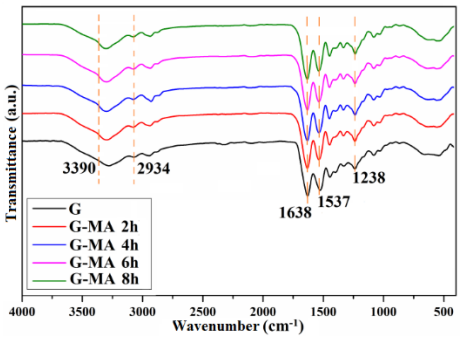

Figure 21. FTIR spectra of gelatin and methacrylated gelatin for 2/4/6 or 8 hours.

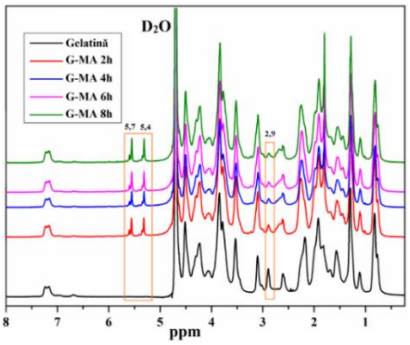

Figure 22. NMR spectra of gelatin and methacrylated gelatin for 2/4/6 or 8 hours.

2.2.3. Preparation and physicochemical characterization of hydrogels

The preparation of hydrogels composed of cellulose derivatives and methacrylate derivatives of gelatin involved the homogenization of the components, whose gravimetric ratios were well established, after which the photoinitiator – riboflavin (1% relative to the total mass of polymers) was added, with an irradiation time of 30 minutes, at a wavelength of 365 nm. The hydrogels obtained were structurally characterized using FTIR spectroscopy, following the characteristic bands of the components (cellulose derivatives – 3300 cm^{-1} and 2925 cm^{-1} – and aminated and methacrylated gelatin – 1638 cm^{-1}, 1537 cm^{-1} and 1238 cm^{-1}). Analyzing and interpreting the spectra in a similar manner to those previously discussed, it was found that the synthesis of the hydrogels was successfully achieved.

The micrograph of the G-MA 2h hydrogel indicates areas with a uniform appearance and a tendency to form pores. Increasing the degree of gelatin functionalization causes changes in morphology, in particular, the appearance of interconnected micropores of 1-4.2 μm and 1.7-6.5 μm.

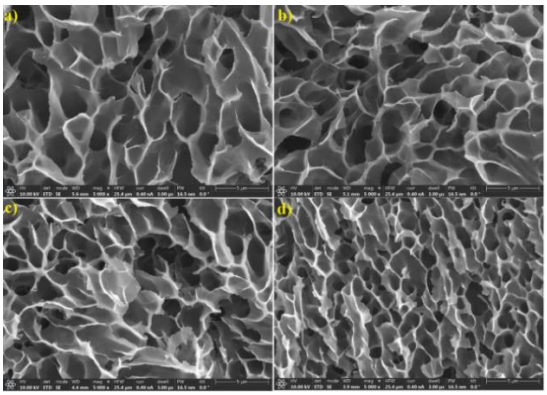

Figure 23. SEM images of hybrid hydrogels: CG 2h **(a)**, CG 4h **(b)**, CG 6h **(c)** and CG 8h **(d)**.

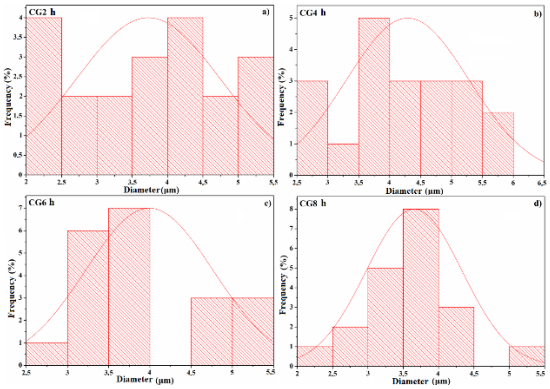

Figure 24. Histograms of the pore diameter distribution of hydrogels CG2 **(a)**, CG4 **(b)**, CG6 **(c)** and CG8 **(d)**.

Comparing the micrographs of the hybrid hydrogels based on C-O-MA and G-MA (at different reaction times), variations in pore size could be observed. Extreme pore values were determined only in the case of the CG 2h hydrogel (**Figure 23a**), being between 2-5 μm. Their appearance is well defined (thin walls), with few areas where they are interconnected. The pores become interconnected with increasing methacrylate degree. The calculated dimensions for the hydrogels in **Figure 24b** and **Figure 24c** are close, 2-5.5 μm, with the specification that the CG 4h hydrogel presents most of the pores over 3 μm, and the CG 8h hydrogel presents pores of similar sizes, most of the pores being ~3-3.5 μm. The SEM micrographs in **Figure 25**

suggest different morphologies of the HPC and gelatin-based hydrogels compared to the others. The porosity of the hydrogels is not well defined, especially in the case of samples with a higher degree of methacrylate. The pore sizes were 2-3µm for all hydrogels. With an increasing degree of methacrylation of the gelatin, the pores acquire a "hairy" appearance, which is not found in C-O hydrogels and is characteristic of HPC.

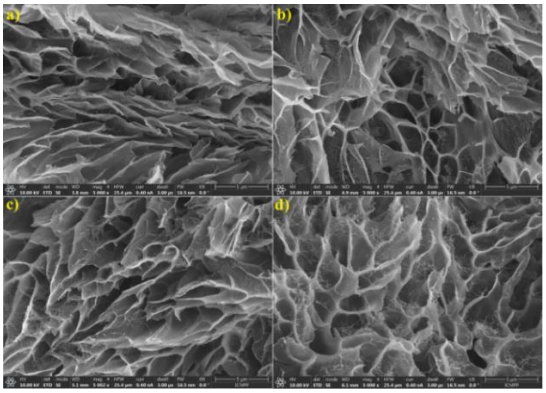

Figure 25. SEM images of hybrid hydrogels: HG 2h **(a)**, HG 4h **(b)**, HG 6h **(c)** and HG 8h **(d)**.

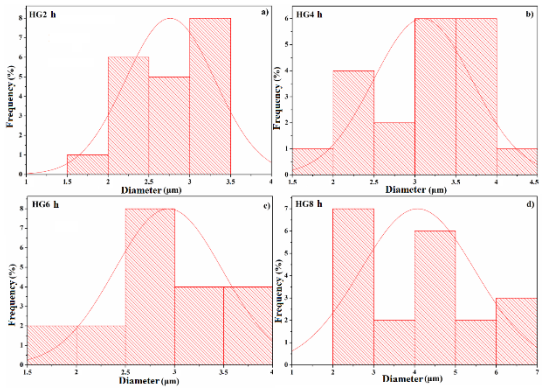

Figure 26. Histograms of the diameter distribution of the pores of hydrogels HG2 **(a)**, HG4 **(b)**, HG6 **(c)** and HG8 **(d)**.

The ability of hydrogels to retain water gives them properties similar to those of living tissues, which is a key advantage for applications in the medical field. The first hydrogels analyzed were those of methacrylic derivatives of gelatin, being considered reference materials, the results being compared with those of hydrogels composed of G-MA and polysaccharide derivatives. The behavior of the G-MA 2h and G-MA 6h hydrogels (**Figure 27a,c**) turned out to be similar, they encapsulated a large volume of water compared to the G-MA 4h and G-MA 8h hydrogels (**Figure 27b,d**), where a limit can be more easily observed. Unlike the other hydrogels, the mass-time curves of G-MA 4h and G-MA 8h illustrate a constant increase in mass according to the immersion time. Correlating with the SEM analysis, it can be deduced that the changes in porosity, depending on the time of the gelatin methacrylate reaction, determine that the hydrogels adopt different liquid absorption behaviors. The mass-time curves corresponding to the C-O-MA and G-MA-based hydrogels are similar to those of the control hydrogels. **Figure 27a-c** shows the evolution over time of the water absorption capacity for hydrogels containing G-MA 2h, G-MA 4h or G-MA6h. The similarity of the curves can be justified by the size of most of the pores (2-5.5 µm). In contrast, the CG 8h hydrogel is porous, with pores similar to those of the hydrogels from the same series of chemical reactions, however, the pore sizes are close (~3 µm), which may contribute

to reaching an absorption threshold. Another explanation refers to the adoption of a behavior similar to the control hydrogel (G-MA 8h). The HG series hydrogels seem to behave differently from the control or CG-based hydrogels, in the sense that they reach an absorption limit around minute 50, the plateau continuing until the end of the measurements. This behavior could be justified by the pore sizes calculated based on SEM images (2-3 μm for each hydrogel, as in the case of CG 8h) and the "hairy" appearance acquired with increasing methacrylate time.

The hydrogels prepared from the compounds synthesized in the previously presented steps were designed to have potential applications in the medical field, precisely due to their properties, especially injectability. To further confirm a possible application in the biomedical field, degradation studies were necessary under conditions that mimic human body fluids. Thus, the degradation of the hydrogels in PBS solutions, pH = 7.4, at room temperature was monitored for a period of 30 days. In **Figure 28a**, high values of mass loss can be observed for G-MA 2h and G-MA 4h from the first day of testing, these being followed by G-MA 6h (the remaining mass is similar) and G-MA 8h. During the monitoring period, the mass losses were slightly significant, the results being more evident at the end of the tests, when the smallest losses were noticed in the case of the hydrogel with the methacrylated gelatin component for the longest time (G-MA 8h) due to the stability conferred by the grafting of the methacrylic sequences. The G-MA 2h and G-MA 6h hydrogels disintegrate completely (G-MA 2h) or almost completely, the remaining mass in the case of G-MA 6h being 12.9% of the initial mass. This can be justified by the interconnected pores, which are not very well delimited. **Figure 28b** illustrates the time evolution of hydrogels based on gelatin or chemically modified cellulose. In this case, the methacrylic gelatin in the composition of the hydrogels imprints its character, thus influencing their degradation differently. The long times of the gelatin methacrylation reaction provide mechanical resistance, but, with the attachment of the methacrylic sequences, the network of physical interactions is thinned, and the hydrogels degrade more easily in the PBS solution. The CG 8h hydrogel disintegrates quickly from the first day, reaching almost total disintegration on the last day (99.2%), while CG 4h and CG 6h have a more staged degradation, with the final masses being 6.4% and 7.8%. All HPC-based photocrosslinked hydrogels gradually disintegrate over the 30 days, as can be seen from **Figure 28c**, but HG 4h and HG 6h ultimately have the lowest mass percentage (27.1% and

21.2%). In conclusion, in the early phase of the study (the first five days), the highest mass losses were identified in the case of G-MA 2h, G-MA 4h and HG 8h hydrogels, and the C-O-MA-G-MA series hydrogels were degraded the slowest, except for the G-MA 8h and C-O-MA-based hydrogel where drastic mass losses occur from the first day. After 30 days, it was found that the CG series hydrogels suffered the greatest degradation, followed by the HG and G-MA hydrogels. Following the aspects discussed, it was concluded that the investigated samples present good biodegradability, which varies depending on the morphology of each hydrogel, large or interconnected pores, determining their more accelerated degradation [114].

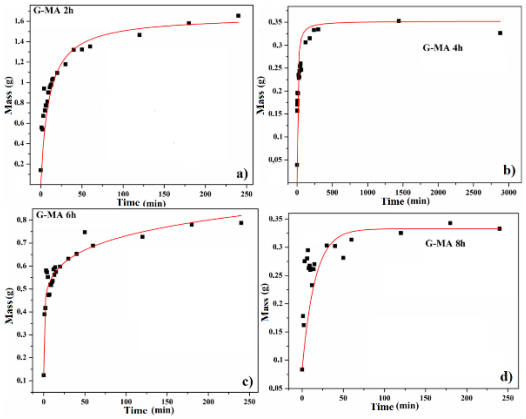

Figure 27. Mass/time curves of control hydrogels G-MA 2h **(a)**, G-MA 4h **(b)**, G-MA 6h **(c)** and G-MA 8h **(d)**.

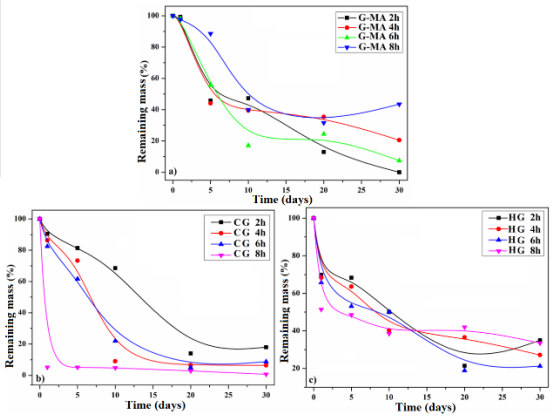

Figure 28. Degradation studies of hydrogels from the G-MA, CG and HG series, in PBS solution, pH = 7.4.

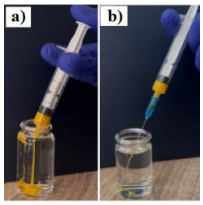

Figure 29. Demonstrative images of the injectability properties of HPC-O-MA-G-MA 4h **(a)** and C-O-MA-G-MA 4h **(b)** hydrogels.

Injectability studies were performed before photocrosslinking. By applying pressure to the syringe plunger, the hydrogels pass through the needle, facilitating their injection.

2.2.5. Conclusions

The synthesized photocrosslinked hydrogels have in their composition cellulose derivatives, obtained by oxidation and methacrylation reactions, and methacrylic derivatives of gelatin. After investigating the chemical structures using FTIR and NMR spectral techniques, the following analyses aimed at investigating the morphology, water absorption capacity and degradation rate, due to the fact that these tests can confirm the potential of

hydrogels to be used in biomedical applications. The study of the morphology of the hydrogels, which correlates with the degradation tests, showed that the size and appearance of the pores influence the degradation rate of the hydrogels in PBS solution, pH = 7.4. The hydrogels whose degradation was gradual and almost complete were the control hydrogel G-MA 2h and the hydrogels based on HPC-O-MA or C-O-MA and the gelatin derivative methacrylate 4 or 6 hours, these being more suitable for medical applications. The last very important test carried out was the one that verified and demonstrated the injectability properties of the hydrogels before irradiation.

2.3. Hydrogels based on oxidized derivatives of cellulose or pullulan, functionalized with aromatic amines

2.3.1. Design of hydrogels

The experiments found in this subchapter involved the functionalization of polysaccharides recognized for their impressive properties: cellulose and pullulan.

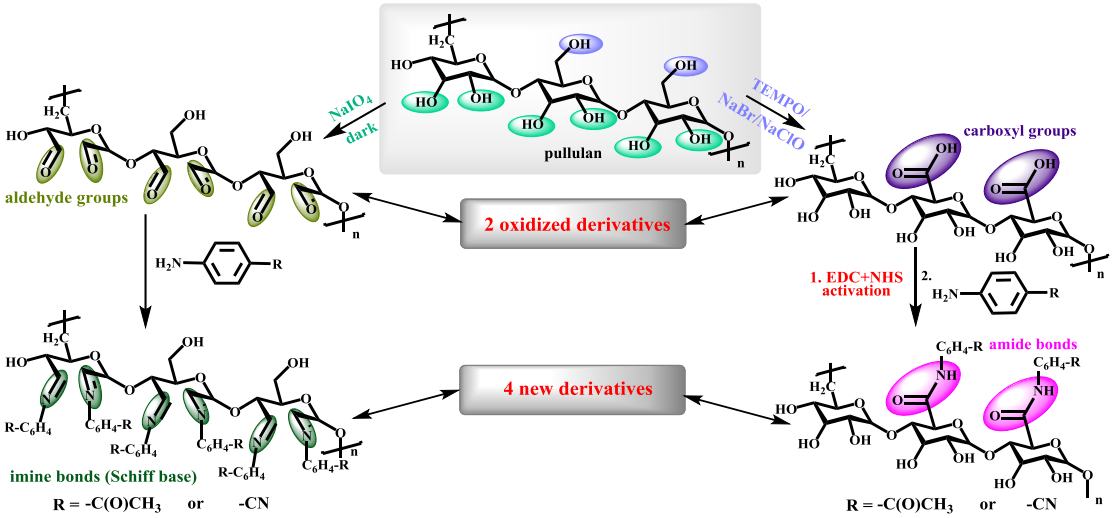

Figure 30. Schematic representation of the syntheses of pullulan derivatives through oxidative reactions, followed by the coupling of amine derivatives.

The functionalization reactions of these polysaccharides consisted of oxidation with selective oxidizing agents (TEMPO, NaClO and NaBr, or $NaIO_4$), the products being subsequently involved in coupling reactions with aromatic amines that presented a dual functionality, such as ketone or nitrile groups (4-aminoacetophenone, 4-AAPh and 4-aminoacetonitrile, 4-ABN). The novelty of the series of reactions came from carrying out these coupling reactions.

Table 2. The synthesized pullulan derivatives and the type of reaction by which they were obtained.

Sample	Chemical reaction to obtain pullulan derivatives
P-OT	Pullulan oxidation reaction in the presence of TEMPO/NaClO/NaBr
P-OT-CH_3	Coupling reaction of oxidized pullulan with TEMPO (P-OT) and 4-aminoacetophenone
P-OT-CN	Coupling reaction of oxidized pullulan with TEMPO (P-OT) and 4-aminobenzonitrile
P-OP	Pullulan oxidation reaction in the presence of $NaIO_4$
P-OP-CH_3	Coupling reaction of oxidized pullulan with $NaIO_4$ (P-OP) and 4-aminoacetophenone
P-OP-CN	Coupling reaction of oxidized pullulan with $NaIO_4$ (P-OP) and 4-aminobenzonitrile

2.3.2. Physico-chemical characterization of hydrogels

The oxidized pullulan derivatives present characteristic pullulan bands such as those at 3500 cm^{-1} corresponding to hydroxyl groups, but also present bands characteristic of grafted sequences. By interpreting the spectra, it can be confirmed that the oxidation reaction in the presence of the TEMPO radical was successfully carried out, as evidenced by the decrease in intensity of the band at 2925 cm^{-1}, attributed to methylene groups and the appearance of the sharp band at 1417 cm^{-1}, characteristic of the vibrations of the C-O bonds of the carboxyl groups. The success of the oxidation reaction in the presence of $NaIO_4$ is demonstrated by the appearance in the P-OP spectrum of the band at 1735 cm^{-1}, corresponding to the vibrations of the C=O bonds of the aldehyde groups formed.

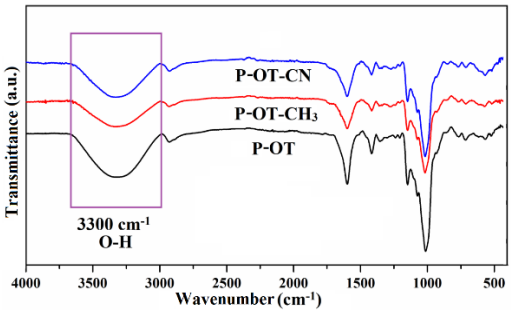

Figure 31. FTIR spectra of P-OT and its derivatives obtained by coupling.

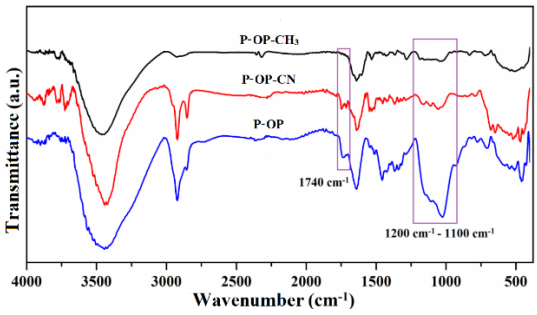

Figure 32. FTIR spectra of P-OP and its derivatives obtained by coupling.

From the FTIR spectra presented in **Figure 31**, a slight change in the intensity of the bands at 3300cm^{-1} and 1413 cm^{-1} corresponding to the carboxylic groups is observed, indicating that the coupling reactions have proceeded accordingly. The FTIR spectra of the P-OP derivatives (**Figure 32**) indicate a decrease in the absorption band at 1740 cm^{-1} characteristic of the aldehyde groups, this fact being due to the coupling reactions and the

formation of imine bonds. The band attributed to the nitrile group is found in the spectrum of the P-OP-CN compound at 2254 cm^{-1}.

2.3.3. Applications – determination of the detection capacity of metal ions in polluted waters by the pullulan derivative with nitrile groups

The applications described in this subchapter aimed at exploring the fluorescent properties of the P-OP-CN derivative due to its structure (nitrile groups, imine bonds and aromatic rings) [117].

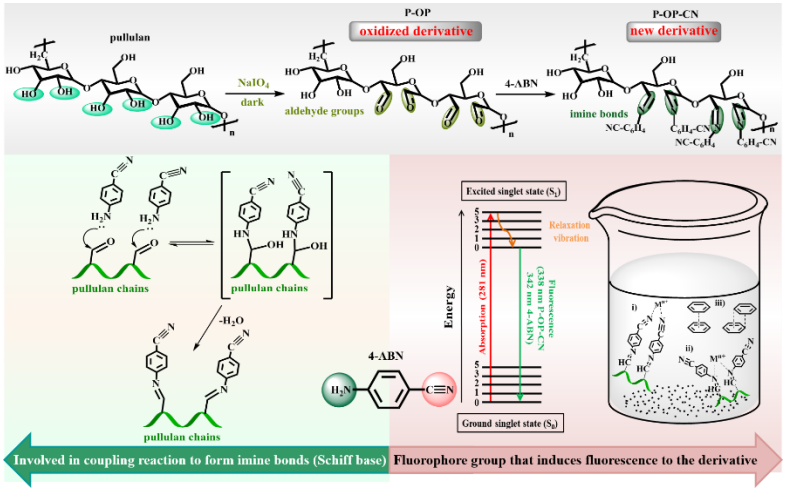

Figure 33. Schematic representation of the synthesis of the P-OP-CN derivative and the structural features that confer fluorescent properties.

The P-OP-CN derivative is a promising fluorescent compound due to the nitrile groups, benzene rings and imine bonds formed by grafting 4-ABN. The limited reporting in the specialized literature of polysaccharides with fluorophoric sequences, studies being carried out mostly on dextran, cellulose and chitosan derivatives, had a significant contribution in carrying out the current study [121,122]. A first preliminary step in determining the fluorescence properties of the samples was to identify the appropriate solvent in which the P-OP-CN samples and the grafted compound could be dissolved. First, the UV spectra of 4-ABN solutions in DMSO and DMF were recorded (**Figure 34**), and following their interpretation it was found that the chosen solvent and the concentration of the solutions are correlated. The absorption band for 4-ABN in DMSO, identified at 281 nm and has the absorbance ~1 when the solution concentration is 0.003 g/L [123]. After investigating the 4-ABN solutions, the functional pullulan derivative, P-OP-CN, was analyzed in order to observe its behavior in organic solvents. In the case of both P-OP-CN solutions, in order to record absorbances with values of ~1, dilutions were made such that the final concentrations were 0.04 g/L (DMF) and

0.03 g/L (DMSO). Comparing the UV spectra of the compounds solubilized in both DMSO and DMF, and correlating them with the concentrations of the solutions, it can be seen that 4-ABN absorbs the strongest, followed by P-OP-CN. The solubilization of the polymer is more efficient in DMSO, and the resulting solution (0.03 g/L), for which the absorbance was determined to be 1, was analyzed to observe whether it possesses fluorescence properties. From the UV spectra, it was observed that both nitrile derivatives exhibit the maximum of the absorption band at 281 nm, and ʎ was used for excitation in fluorescence experiments, respectively, to determine the emission band in the fluorescence spectra and to evaluate the fluorescence intensity of the P-OP-CN compound compared to that of 4-ABN. Even though the absorption band appeared at the same wavelength, the emission bands, different in intensity and shape, are found at different wavelengths: 342 nm (4-ABN) and 338 nm (P-OP-CN), **Figure 36**. The pullulan derivative has stronger fluorescent properties than 4-ABN, most likely due to the 4-ABN sequences – a light-sensitive compound that becomes stable by grafting onto the polymer chains, disabling decomposition when the polymer derivative is exposed to light radiation.

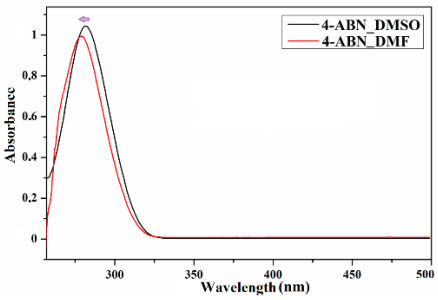

Figure 34. UV spectra of 4-ABN in DMSO and DMF.

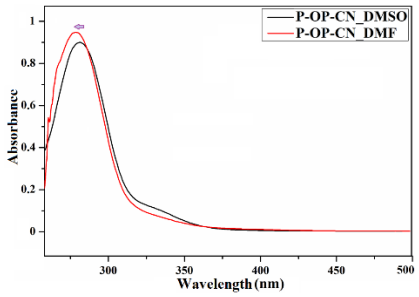

Figure 35 UV spectra of P-OP-CN in DMSO and DMF.

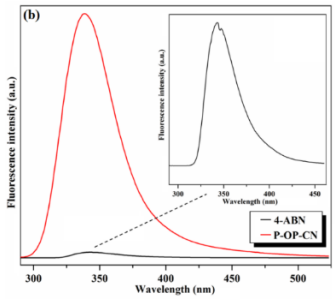

Figure 36. Fluorescence spectra of P-OP-CN and 4-ABN in DMSO.

There are physical or chemical processes that influence the fluorescence of a compound (formation of coordination compounds, energy transfer), in the sense that they can reduce (quench) or increase (light up) its intensity. The processes that can occur following the addition of solutions of compounds with low molecular masses, such as metal ions from metal salts. Therefore, the fluorescence of the P-OP-CN derivative was evaluated when it was analyzed individually and in combination with metal ions (aqueous solutions). The metal ions chosen in this analysis were Mn^{2+}, Fe^{3+}, Fe^{2+}, Ni^{2+}, Cu^{2+}, Zn^{2+}, Ag^{+}, Cd^{2+}, Hg^{2+}, Pb^{2+}, Na^{+} and Ca^{2+}, their solutions being made in distilled water (3×10^{-3} M). The emission spectra of P-OP-CN in DMSO (0.03g/L), recorded at a fixed quenching concentration and an excitation

wavelength of 281 nm, provide an emission band at 338 nm, given by the benzonitrile units. In general, no changes were observed in the positions and shapes of the fluorescence bands, except for the intensity at which the band maxima are found, implicitly the fluorescence intensity of P-OP-CN, which decreased drastically with increasing quenching concentrations.

Table 3. The main parameters determined after quenching the fluorescence exhibited by P-OP-CN with aqueous solutions of metal ions.

Metal ion	Limit of detection $\times 10^{-5}$ (M)	Quenching degree (%), 600×10^{-6} M	k_{SV} ($\times 10^6$ M^{-1})	k ($\times 10^6$ M^{-1})
Fe^{3+}	0.189	100	0.83333 (R^2=1)	-
Cu^{2+}	0.340	95.67	0.01123 (R^2=0.986)	0.0044 (R^2=0.977)
Fe^{2+}	0.735	62.48	0.00515 (R^2=0.996)	0.0067 (R^2=0.997)
Pb^{2+}	6.042	51.62	0.00315 (R^2=0.986)	0.0052 (R^2=0.994)
Hg^{2+}	2.964	50.35	0.00217 (R^2=0.989)	0.0016 (R^2=0.993)
Ca^{2+}	2.042	49.47	0.00169 (R^2=0.995)	-
Mn^{2+}	6.638	47.57	0.00144 (R^2=0.999)	-
Ag^{+}	3.305	46.98	0.00134 (R^2=0.988)	0.0009 (R^2=0.999)
Cd^{2+}	2.428	46.11	0.00151 (R^2=0.990)	-
Ni^{2+}	2.943	45.05	0.00125 (R^2=0.991)	0.0012 (R^2=0.989)
Zn^{2+}	3.821	41.84	0.00091 (R^2=0.994)	0.0008 (R^2=0.999)
Na^{+}	3.171	36.00	0.00069 (R^2=0.989)	0.0002 (R^2=0.997)

The data presented in **Table 3** indicate that the Fe^{3+} ion is the most suitable quencher for this polymer, allowing it to quench the fluorescence in 100% percentage before the P-OP-CN+Fe^{3+} solution reaches 600×10^{-6} M. The most efficient quenching after Fe^{3+} is had by Cu^{2+} (fluorescence reduction up to 95.67%, c = 600×10^{-6} M). Regarding the fluorescence quenching at a fixed concentration, the decreasing order of excellence of all cations is as follows: Fe^{3+}>Cu^{2+}>Pb^{2+}>Hg^{2+}>Ca^{2+}>Mn^{2+}>Ag^{+}>Cd^{2+}>Ni^{2+}>Zn^{2+}>Na^{+}. The mechanism by which the fluorescence quenching by metal ions occurs was investigated by performing Stern-Volmer plots. A linear relationship suggests the dynamic behavior of the quenching mechanism, characterized by the Stern-Volmer constant (k_{SV}), as a result of interactions between the added cations and the fluorophore groups of the polymer in the excited state. If the plot shows a curve, this highlights that the quenching is achieved by a mixed (dynamic-static) mechanism, the static mechanism involving the formation of a complex devoid of fluorescent properties. **Figure 37a** shows the fluorescence spectra of the P-OP-CN solution before and after the addition of the Fe^{3+} solution. After the addition of 100 μL of quencher solution (120×10^{-6} M), the calculated GS(%) was 95.97%. From the concentration versus I_0/I plot, **Figure 37b**, it can

be seen that the fluorescence quenching by Fe^{3+} occurs through a dynamic mechanism over the entire range (k_{SV}=0.8333×10^6 M^{-1}, estimated from the slope calculated at λ=338nm; R^2=1).

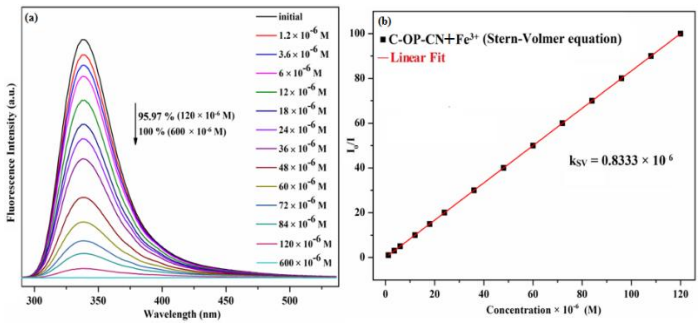

Figure 37. Fluorescence spectra of P-OP-CN solution in the presence of Fe^{3+}, at different concentrations **(a)** and Stern-Volmer plot **(b)**.

The fluorescence quenching of P-OP-CN with Cu^{2+} solution is represented in **Figure 38a**, where it is observed that, at a higher concentration, the emission band shifts slightly to the right (~1-2 nm), showing a bathochromic effect. Thus, a different Stern-Volmer plot can be observed in this case (**Figure 38b**), having the appearance of a curve, implicitly a dual behavior of the quenching mechanism. Thus, the Stern-Volmer plot was modified to include only the concentrations from the initial one to 60×10^{-6} M, which provides a linear relationship with I_0/I (k_{SV} = 0.01123×10^6 M^{-1}, estimated from the slope and R^2 =0.986, at λ=338 nm), while the Lehrer plot included the rest of the concentrations (k = 0.0044×10^6 M^{-1} at λ=341 nm; R^2 = 0.977). Considering the appearance of the curve (positive deviation from linearity), the predominant mechanism is the static one.

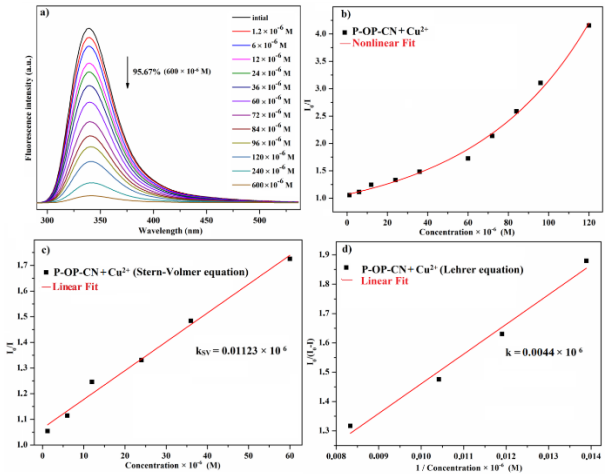

Figure 38. Fluorescence spectra of the P-OP-CN solution in the presence of Cu^{2+}, at different concentrations **(a)**, the Stern-Volmer plot for all concentrations of the P-OP-CN+Cu^{2+} solution **(b)**, for concentrations up to 60×10^{-6} M **(c)** and the Lehrer plot **(d)**.

The chemosensor activity was determined by studying the competitive selectivity of P-OP-CN for Fe^{3+} and Cu^{2+}, the tests being performed in the presence of different ions at the same concentration to certify the ability of P-OP-CN to resist the interference of other competing metal ions. At the same amount of quencher (100 µL, 3×10^{-3} M), P-OP-CN showed excellent selectivity for Fe^{3+} among all metal ions.

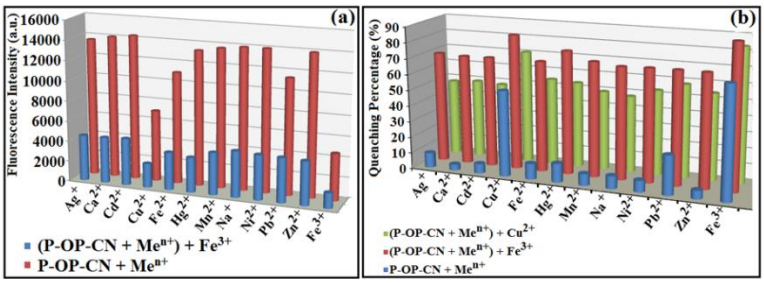

Figure 39. Competitive studies **(a)** and GS(%) of the fluorescence of the P-OP-CN compound in the presence of various cations, before and after the addition of 100 µL Fe^{3+} / Cu^{2+} **(b)**.

The formation of coordination compounds involves the electrostatic interaction between the lone pairs of electrons from the nitrogen atom of the nitrile (–C≡N) terminal groups in the polymer, which can act as ligands in the interaction with metal ions that act as electron acceptors due to their positive charge. The stoichiometry of the complex formed between P-OP-CN and Fe^{3+} was determined by the Job plot, indicating the changes in the intensity of the fluorescence bands at 338 nm as a function of the molar fraction of Fe^{3+}. The molar concentration of the P-OP-CN polymer was calculated considering the maximum degree of functionalization as revealed by the interpretation of the ^{1}H-NMR spectra of P-OP and P-OP-CN, indicating that most of the aldehyde groups were converted into imine groups. The intersection of the lines at 0.33 suggests a stoichiometric ratio of 1:2 between P-OP-CN and Fe3+ [125]. The association between the polymer and Fe^{3+} or Cu^{2+} was investigated by determining the polymer-metal ion bond strength, information provided by the value of the association constants (k_a), determined from the modified Benesi-Hildebrand plot, also indicating the speed of the process. Considering the efficient quenching properties of Fe^{3+} ions, the highest k_a value was obtained for the P-OP-CN+Fe^{3+} system (28.16×10^{3} M^{-1}), followed by the P-OP-CN+Cu^{2+} system (24.51×10^{3} M^{-1}).

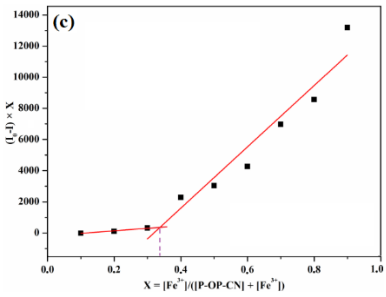

Figure 40. Graph of fluorescence titration with Fe^{3+} as a function of mole fractions.

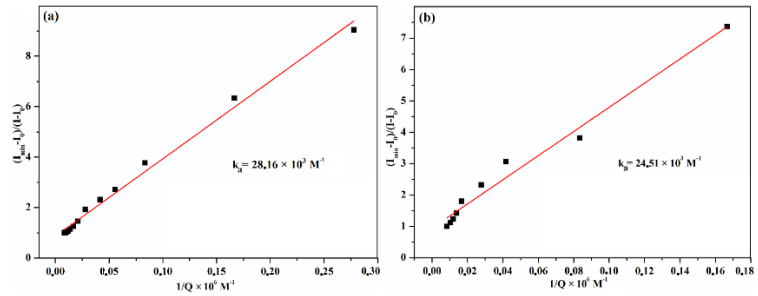

Figure 41. Benesi–Hildebrand plot for the determination of k_a attributed to the complexation of P-OP-CN with Fe^{3+} **(a)** and Cu^{2+} **(b)** at 120 × 10^{-6} M.

The UV spectra of all compound solutions (with 100 µL of quencher solution) were recorded and compared with the spectrum of the blank solution. Most of the mixed solutions have a similar behavior to the blank solution, their absorption bands being at the same wavelength (~281 nm), but having low intensities.

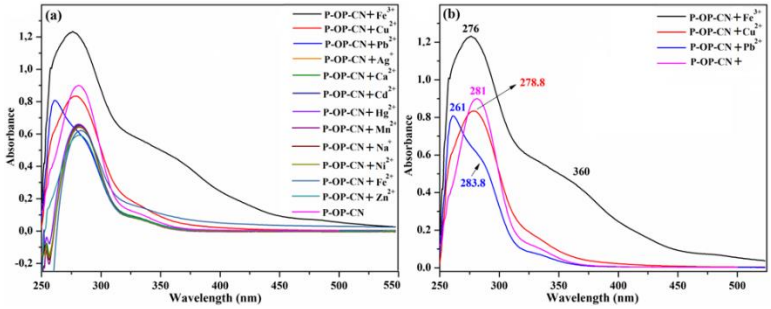

Figure 42. UV spectra of P-OP-CN, before and after the addition of different quenchers **(a)** and P-OP-CN mixed with the most effective quenchers (Fe^{3+}, Cu^{2+} and Pb^{2+}) **(b)**.

Solutions composed of polymer and Fe^{3+}, Cu^{2+} or Pb^{2+} show changes in the bands in terms of ʎ or aspect. Both polymer+Pb^{2+} and polymer+Fe^{3+} bands have different intensities compared to the control solution and show a peak like shoulder on the right side at 283.8 nm (Pb^{2+}) and 360 nm (Fe^{3+}), and the maxima undergo hypsochromic shifts at 261nm (Pb^{2+}) and 276nm (Fe^{3+}). The polymer+Cu^{2+} solution shows a slight decrease in absorbance intensity and a shift towards lower wavelength values (278.8 nm). In the case of the P-OP-CN+Fe^{3+} solution, the changes in band position and intensity are most likely due to an intramolecular charge transfer of P-OP-CN due to electronic conjugation resulting from ion binding [126].

2.3.5. Conclusion

The aims of these experiments consisted in broadening the scope of existing polysaccharide derivatives by grafting some functions onto the polymer chains and in investigating the modifications undergone by polysaccharides. Before grafting some functions

through coupling reactions, polysaccharides participated in oxidation reactions with selective agents that led to the synthesis of different oxidized derivatives, with carboxyl or carbonyl groups of aldehyde type. In addition to modifying the properties, grafting reactions offered possibilities for the synthesized derivatives to be involved in applications with practical potential. Thus, the compounds chosen to be grafted, being aromatic amines and also having nitrile or ketone groups in the chemical structure, allowed opening up possibilities for their subsequent use in photochemical applications involving the detection and capture of metal ions. Among the new derivatives, the P-OP-CN compound stands out by possessing a fluorescent behavior conferred by the structural features resulting from the attachment of the 4-ABN compound. The emission spectrum of the P-OP-CN solution in DMSO solvent, recorded after excitation of the sample at the wavelength (λ) determined from the UV spectrum (281 nm), shows a strong fluorescence. This particularity was investigated when aqueous solutions of metal ions were added to observe the influence of ions recognized for their ability to reduce or enhance the fluorescent character of substances. Changes in fluorescence intensity occurred from the smallest added volume of metal ion solution (1 μL– concentration 1.2×10^{-6} M) to 1000 μL (1200×10^{-6} M), with the exception of Fe^{3+} and Cu^{2+} ions that completely or almost completely quenched the fluorescence around 100 (120×10^{-6} M) and 500 μL (600×10^{-6} M), respectively. In these experiments, all metal ion solutions contributed to the reduction of the fluorescent properties of P-OP-CN, acting as quenchers. Therefore, the quenching mechanism was investigated and it was observed that it differs depending on the quencher solution added. Most of the metal ions act on the fluorescence through a combined mechanism (dynamic-static) according to the Stern-Volmer and Lehrer plots and the values of the constants obtained from the plots, the predominant stage of the mechanism being the static one for all quenchers, except for the Fe^{2+} and Pb^{2+} ions, for which the predominant mechanism is dynamic. However, other ions, including Fe^{3+}, quench the fluorescence by a dynamic mechanism. Of all the ions investigated, the fluorescence is most effectively reduced by the addition of trivalent iron ions, which act only by a dynamic mechanism, as is the case with Mn^{2+}, Cd^{2+} and Ca^{2+} ions. In order to further highlight the effectiveness of Fe^{3+} ions, selectivity studies were performed using solutions of the P-OP-CN polymer in the presence of two metals, the second metal (Fe^{3+}) causing a drastic decrease in fluorescence compared to the first. The fluorescence modification, attributed to the

interactions established between P-OP-CN and the metal ions and leading to the formation of chemical complexes, was studied by representing the Job and Benesi-Hildebrand plots, the interpretation of which provided information about the stoichiometry of the components in the complex (1:2) and the strength of the bond.

2.4. Hydrogels with multiple crosslinks, based on pullulan derivatives, polyvinyl alcohol and 3-aminoboronic acid

2.4.1. Design of hydrogels

The experiments presented in this chapter aimed at obtaining hydrogels with multiple crosslinks that would be endowed with properties specific to biomedical applications. For the design of these hydrogels, we used pullulan derivatives and PVA as components. The functional groups grafted onto the polymer chains provide increased reactivity and are the main reason why we opted for pullulan derivatives instead of the basic polysaccharide. To obtain the hydrogels, two polysaccharide derivatives were used: carboxypullulan (obtained by oxidation in the presence of TEMPO) and dialdehyde pullulan (obtained by oxidation in the presence of $NaIO_4$). The functionalized derivatives participated in coupling reactions with 3-aminophenylboronic acid and subsequently mixed with the PVA solution, in different ratios.

Table 5. Gravimetric ratios between components of hydrogels of P and T series.

T_1 = P-OT-PVA		**T_2 = P-OT-BA-PVA**	
P-OT	**PVA**	**P-OT-BA**	**PVA**
25	75	25	75
50	50	50	50
75	25	75	25
P_1 = P-OP-PVA		**P_2 = P-OP-BA-PVA**	
P-OP	**PVA**	**P-OP-BA**	**PVA**
25	75	25	75
50	50	50	50
75	25	75	25

T series: P-OT= pullulan oxidized in the presence of TEMPO; **P-OT-PVA**= hydrogel based on P-OT and PVA; **P-OT-BA**= pullulan derivative obtained by the coupling reaction between P-OT and 3-aminophenylboronic acid (3-BA); **P-OT-BA-PVA** = hydrogel based on P-OT-BA and PVA

P series: P-OP= pullulan oxidized in the presence of $NaIO_4$; **P-OP-PVA** = hydrogel based on P-OT and PVA; **P-OP-BA** = pullulan derivative obtained by the coupling reaction between P-

OP and 3-aminophenylboronic acid (3-BA); **P-OP-BA-PVA** = hydrogel based on P-OP-BA and PVA

The crosslinks in the P and T series hydrogels are physical and chemical crosslinks, found only in one of the series or in both. **Figure 43** illustrates the chemical structures of the precursors of the P series hydrogels, the synthesis methods (obtaining hydrogels P1 and P2), but also the types of crosslinks formed between the functional groups of the chosen polysaccharide derivative and PVA. Thus, in the P1 series, hydrogen bonds and (hemi)acetal bonds are identified between the alcoholic groups in PVA and the aldehyde groups in P-OP. The existence of these bonds is unlikely in the case of the P2 series because the grafted 3-BA residues are bulky and prevent their formation, instead, new ester chemical bonds may appear between PVA and the 3-BA sequences in P-OP (P-OP-BA is considered a Schiff base compound due to the 3-BA sequences grafted through imine bonds). Similar to P1 and P2 hydrogels, T-series hydrogels (**Figure 44**) contain physical interactions. Between the PVA chains and the carboxylic groups formed in pullulan by oxidation reactions, chemical crosslinks are formed – ester bonds originating from carboxylic acids. T2 series also contains ester bonds, but these originate from 3-BA, although there could also be bonds formed between the unreacted -COOH groups and PVA.

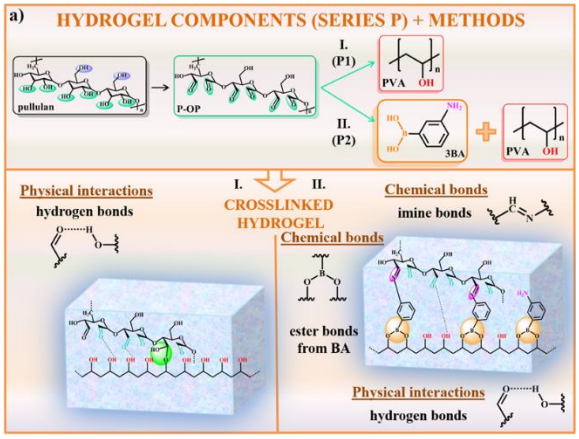

Figure 43. Representative diagram of the components of P-series hydrogels.

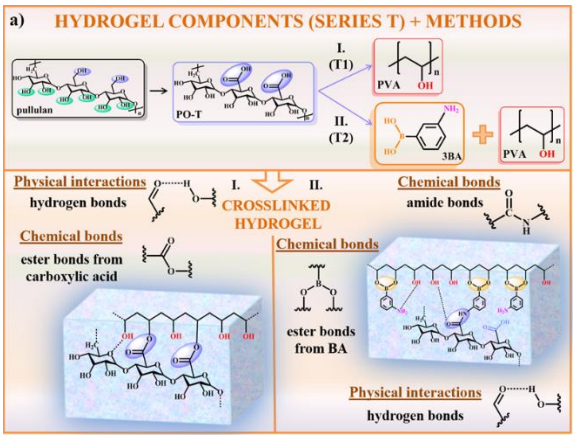

Figure 44. Representative diagram of the components of T-series hydrogels.

2.4.2. Physico-chemical characterization of hydrogels

The characterization of the hydrogels was first carried out by spectral methods. **Figure 45** shows the FTIR spectra of the initial compounds that were used to obtain the corresponding hydrogels. From the FTIR spectrum of the P1 series (**Figure 46**) it is assumed that the different gravimetric ratios between P-OP and PVA affect the intensity or shift of the bands.

Slight changes occur in the case of the P1 50-50 compound whose spectrum undergoes changes in the band at 3300 cm^{-1}, characteristic of hydroxyl groups. This may be a consequence of the fact that between PVA and the oxidized pullulan derivative a number of intrachain hydrogen bonds are created proportional to that of the interchain bonds formed, unlike P1 25-75 and P1 75-25. Also, at 837 cm^{-1} the characteristic band for PVA appears, this being more evident in the spectrum of the hydrogel predominantly composed of PVA (P1 25-75). In contrast, in the case of all compounds, the band at ~1030 cm^{-1} represents a shift of the characteristic band at 1092 cm^{-1} for PVA, the greatest similarity, in terms of intensity and allure, being between PVA and the P1 75-25 hydrogel. In addition to the bands corresponding to the groups in PVA and P-OP, characteristic of the P2 hydrogel series are also the bands assigned to the groups originating from the boronic acid derivative which are found in the FTIR spectrum between 400-710 cm^{-1} (B-O, B-C vibrations) and 1596 cm^{-1} (C-H vibrations from the aromatic nucleus).

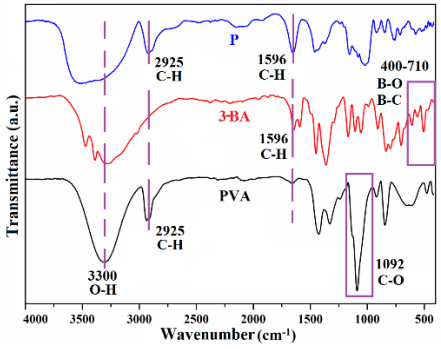

Figure 45. ATR-FTIR spectra of compounds: P, 3-BA and PVA.

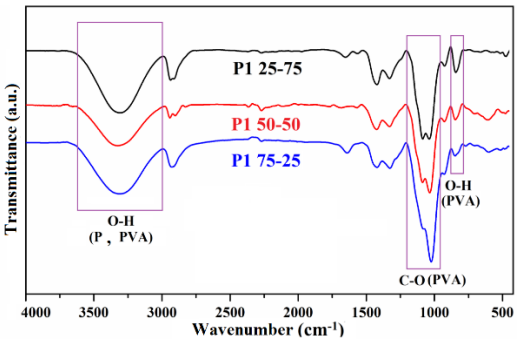

Figure 46. ATR-FTIR spectra of hydrogels from P1 series.

The NMR spectrum of P-OT-BA shows peaks in the aliphatic region from pullulan units and oxidized product, but also new peaks such as that of the amide proton at 7.4 ppm. Further evidence is represented by the signals at 6.7-7.2 ppm of the aromatic protons of 3-BA.

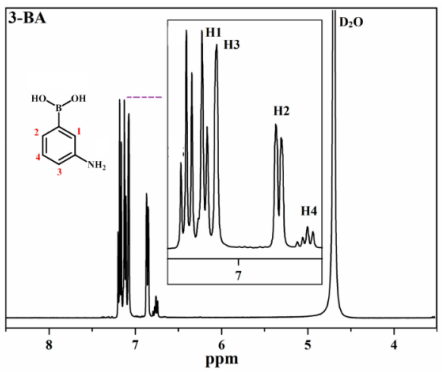

Figure 47. ^{1}H-RMN spectrum of 3-aminophenylboronic acid (3-BA).

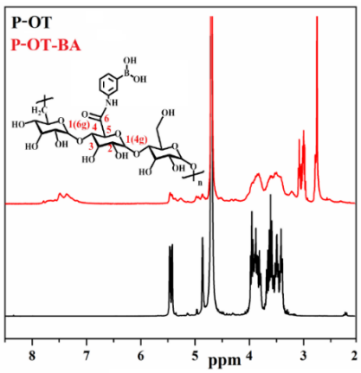

Figure 48. ^{1}H-RMN spectra of compounds: P-OT and P-OT-BA.

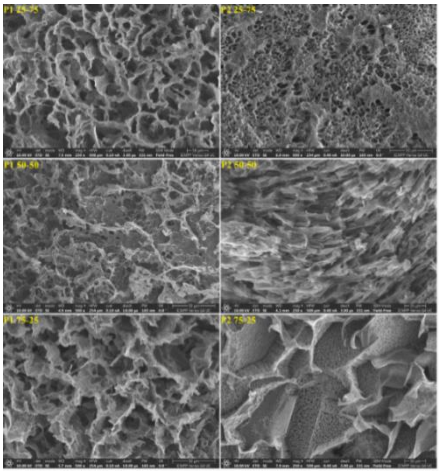

Figure 49. SEM micrographs of hydrogels from P1 and P2 series.

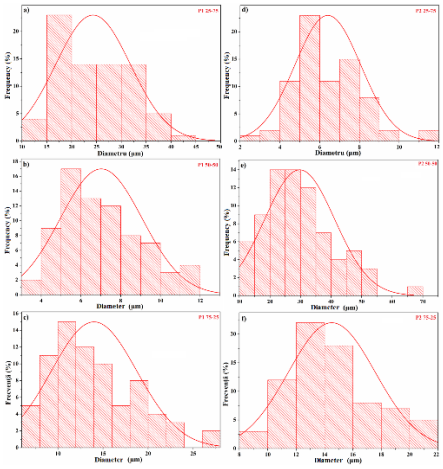

Figure 50. Diameter distribution histograms of the pores of hydrogels from series P1 and P2.

Following the analysis of SEM micrographs, it was found that different gravimetric ratios of the components in the hydrogels determine morphological changes. Grafting of 3-BA sequences contributes to changing the pore size, respectively their distribution. However, the composition and homogeneous distribution of the pores suggest that these components are well compatible. The two series of hydrogels present interconnected pores that would allow the absorption of liquids, making them preferred candidates for biological applications. Hydrogels with a high content of polysaccharide derivative present pores of smaller sizes than those in which the ratio is equal or the major component is PVA.

Through the investigation of the "swelling capacity", the mass/time curves were obtained, which resulted in three different behaviors of the P and T series hydrogels. The different gravimetric ratios between the components and the nature of the existing crosslinks exert their influence on the swelling capacity, which either varies from one sample to another or adopts a similar character. The degradation of the P2 25-75 and T2 25-75 samples occurs at ~178 minutes. In **Figure 51b**, a plateau is observed around 60 minutes, contrary to **Figure 51a** when the maximum water absorption is reached immediately before the decomposition begins. The close results can most likely be justified by the fact that the samples have the identical modified pullulan/PVA gravimetric ratio and contain crosslinks formed by the grafted sequences of 3-BA. The stability of the P2 50-50 and T2 75-25 hydrogels (**Figure 52**) in water is almost non-existent, with the P2 50-50 sample being more resistant to contact with water and completely degrading in 9 minutes, while the T2 75-25 sample is decomposed in just 5

minutes after immersion. High instability is encountered in the case of the P2 75-25 hydrogel for which mass variations following water absorption could not be determined, it completely decomposed from the first measurement. An important consideration for which these hydrogels are unstable is that the hydrogels are more rigid and brittle, as a result of a low PVA ratio (which provides flexibility). Following the results obtained, it can be appreciated that the T2 75-25 hydrogel, in which the gravimetric ratio of carboxylic pullulan is higher than that of PVA, has the best absorption capacity, but its degradation occurs very quickly. Also, the hydrogels T1 25-75 and T1 50-50 have good absorbent properties, and their degradation occurs partially, after a long time. Among all the hydrogels of the P series, a remarkable absorption capacity is that of the hydrogel with a higher gravimetric ratio of pullulan dialdehyde to PVA, P2 75-25 (which contains ester bonds from boronic acid). However, measurements could not be made for this one, its degradation being total and extremely fast (a few seconds). Thus, we can deduce that the bonds made with 3-BA improve the absorption of liquids, but in the short term, since these hydrogels degrade the fastest. Other hydrogels of the P series with a good swelling capacity are P1 25-75 and P1 75-25.

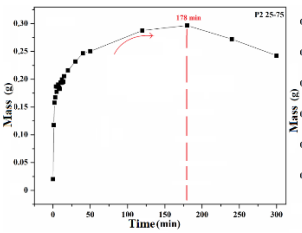

Figure 51. Mass/time curves of hydrogels P2 25-75 **(a)** and T2 25-75 **(b)**.

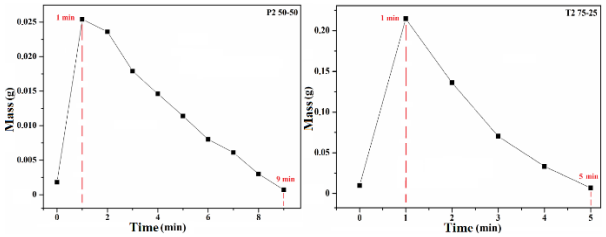

Figure 52. Mass/time curves of hydrogels P2 50-50 **(a)** and T2 75-25 **(b)**.

Information on the volume, density and porosity was obtained for each hydrogel in the wet state. Assuming that ρ was determined in percentages, it can be seen that there are similar values for ρ and P(%) for all hydrogels (**Figure 53**). The XRD spectrum of the PVA hydrogel was compared with the spectra of hydrogels from the P and T series, which have the highest PVA content. The peaks attributed to alcohol are found in the PVA spectrum at 19.6°, 22.6° and 40.8° and correspond to crystalline zones due to the multitude of hydrogen bonds between the alcohol groups [131]. Each hydrogel has a different crystallinity from the others, decreasing in the order: PVA> T2 25-75 >P2 25-75 > T1 25-75 > P1 25-75.

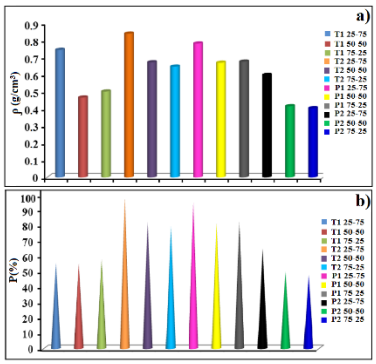

Figure 53. Density **(a)** and porosity **(b)** of hydrogels in wet state.

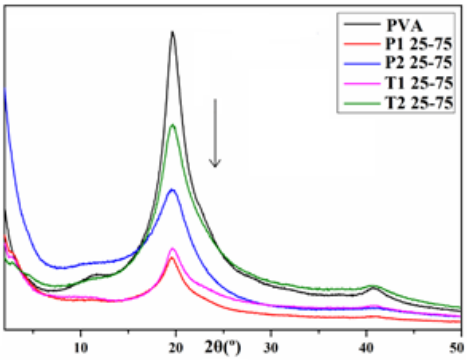

Figure 54. XRD spectra of PVA and hydrogels (P and T series) with the ratio between the pullulan derivative and PVA of 25-75.

2.4.3. Application – outlooks

Undeniably, in recent years, the research in macromolecular chemistry has involved the development of polymeric materials within the scope of "green chemistry" (the compounds of origin and solvents, chosen to be manipulated in experiments, which must not present toxicity), with impressive and vast properties, allowing their use in several applications. Starting from this aspect, I aimed to expand the experiments carried out in the elaboration of the doctoral thesis and to capitalize on the properties offered by polysaccharides by exploiting their ability to obtain hydrogels, characterized by high porosity. The hydrogels synthesized in this subchapter are materials suitable for applications involving the synthesis of metallic nanoparticles. In **chapter 2.1.** we explained the reasons why their generation from precursors presents a series of advantages over other techniques, and the intention in this chapter is to use them in the future as metal reducing agents in precursors, but also as stabilizing agents for the formed nanoparticles [133]. At the same time, hydrogels can be used in combination with photosensitive compounds to form networks with several types of crosslinking, which allow the inclusion of photocatalyst nanoparticles. Other possible applications involve the use of hydrogels as bioadsorbent materials for organic and inorganic pollutants found in contaminated waters, applications similar to those in **chapter 2.3.**. This may be possible due to the carboxyl groups of oxidized pullulan derivatives, which can capture cationic dyes, but the adsorption capacity must be evaluated taking into account the influence of various parameters such as: pH, type of dye and adsorbent dose [134]. Such studies are already found in the scientific literature, but the novelty of hydrogels refers to the ester bonds derived from 3-

aminophenylboronic acid (reversible bonds), giving the materials good mechanical and chemical properties and a possible application in the biomedical field.

2.4.4. Conclusion

Spectral techniques demonstrated the success of the pullulan oxidation reactions, of the coupling reactions with 3-BA and the formation of hydrogels from PVA and the obtained pullulan derivatives. SEM analysis allowed the investigation of the morphology presented by each hydrogel, and it was possible to observe that they are porous materials, with pore sizes in the order of micrometers. Porosity determination tests were carried out in order to complete the interpretations of the results provided by SEM analysis. The main characteristic to be investigated was the liquid absorption capacity, with the swelling degrees being calculated. Analyzing the obtained values, it was found that, although the ratio of pullulan with 3-BA sequences varies from hydrogel to hydrogel, 3-BA determines a strong liquid absorption, followed by the collapse of the materials, so that it can be concluded that hydrogels without 3-BA sequences are more stable when wet. In conclusion, the studies conducted on T and P series hydrogels are preliminary, and will be rigorously characterized and tested for the proposed applications.

GENERAL CONCLUSIONS

The experiments carried out within this doctoral thesis had the role of putting into practice the notions acquired following the study of the scientific literature in the field of the doctoral thesis, in the field of polysaccharides and photochemistry, with the specification that some established synthesis protocols were adjusted to obtain new polymer compounds and materials. The introductory part, studying the current state of knowledge in the field of the thesis, represented the "starting line" of my scientific journey, meant to bring to the forefront new ideas, concepts and achievements, all of these with the role of satisfying the needs of the contemporary world in areas of great interest, such as biomedical and environmental. As general conclusions of the doctoral thesis, ideas emerge that can be delimited in the chapters dedicated to the practical directions addressed:

Photocrosslinked hybrid nanocomposites based on modified cellulose acetate, cerium oxide and noble metal nanoparticles

- ✓ Photocrosslinked polymer networks were developed based on natural compounds chemically modified to contain photosensitive (methacrylic) groups – cellulose acetate and urethane-methacrylic comonomers (castor oil or polypropylene glycol). Castor oil proved to

be a better comonomer, which is why the organic components used in the preparation of nanocomposites were only a derivative of cellulose acetate and castor oil.

✓ The research subject in this chapter consisted of optimizing the photocatalytic activity of CeO_2 by including it in the synthesized networks with the role of support matrices and testing the photocatalytic efficiency in the degradation of some organic pollutants (brilliant green, rhodamine B, Congo red and 4-nitrophenol).

✓ The nanocomposites, synthesized in the form of polymer films, have organic and inorganic components (CeO_2 and noble metals – Au, Ag, Pd). SEM analysis revealed that the gravimetric ratio between the two organic components is decisive in obtaining the desired properties. Thus, the best photocatalytic efficiency was determined for films in which the ratio between the organic components (cellulose acetate derivative and comonomer) was 50:50 and which contain nanoparticles *in situ* photochemically generated.

✓ Of all the organic pollutants in the photodegradation studies, brilliant green was decomposed the fastest under the action of the F1-CeAg film which proved to be the most effective.

✓ The synthesized nanocomposite films also stand out by maintaining impressive performance, close to 100%, even after multiple cycles of use.

Injectable hydrogels based on cellulose derivatives and gelatin, photochemically crosslinked

✓ Functional derivatives of some cellulosic compounds (cellulose and hydroxypropylcellulose – HPC) and gelatin were synthesized following reactions characteristic of the groups in their structures. Each precursor was subjected to reaction with methacrylic anhydride, notably, the cellulosic compounds required prior oxidation with specific oxidizing agents to create the groups capable of reacting with the anhydride. Thus, cellulose was oxidized in the presence of the TEMPO radical and $NaIO_4$ to convert all hydroxyl groups into carboxyl groups and to cleave the bond between the carbon atoms in the "2" and "3" positions, and HPC was oxidized in the presence of HClO to obtain ketone groups from the hydroxyl ones.

✓ Photocrosslinked hydrogels based on methacrylic cellulose derivatives and the methacrylic derivative of gelatin have been developed. In addition to the crosslinks obtained by photopolymerization, the hydrogel made up of methacrylic derivatives of HPC and gelatin

also presents crosslinks of a chemical nature (imine bonds established between the ketone groups formed and the amine groups of gelatin that did not react with methacrylic anhydride), unlike the hydrogel based on methacrylic cellulose which was obtained exclusively by photochemical crosslinking.

✓ The synthesis of hydrogels in this chapter may have implications in the biomedical field, more specifically in tissue repair, which is why the photocrosslinked hydrogels were tested to determine the water absorption capacity and degradation rate in environments that mimic biological fluids (PBS, pH=7.4), and the mixture of compounds before photopolymerization was tested to determine the injectability properties. It was demonstrated that the prepared hydrogels exhibit excellent absorption and injectability properties. The degradation of hydrogels composed of cellulose derivatives and methacrylated gelatin (4 or 6 hours) was gradual and almost complete, suggesting their potential for use in medical applications.

Hydrogels based on oxidized derivatives of cellulose (C) or pullulan (P), functionalized with aromatic amines

✓ Functional derivatives of cellulose and pullulan were synthesized following oxidation reactions, either in the presence of the TEMPO/NaClO/NaBr system (forming intermediate compounds with carboxyl groups), or in the presence of $NaIO_4$ (forming compounds with aldehyde groups), and coupling reactions between the oxidized derivatives and aromatic amines substituted in the para position (forming compounds with amide or imine groups). Thus, the solubility properties of the polysaccharides were modified, with the cellulose and pullulan derivatives becoming partially, respectively totally, soluble in organic solvents (DMSO and DMF).

✓ The P-OP-CN derivative, obtained by oxidation of pullulan with $NaIO_4$ and coupling reaction of the oxidation product with 4-aminobenzonitrile, is of interest due to its fluorescent properties.

✓ The fluorescent behavior of the compound was further evaluated when solutions of metal ions – known for their ability to modify fluorescent properties – were added to the P-OP-CN solution in DMSO. Numerous metal ions were tested, each acting as a quencher of the polymer's fluorescence, but only Fe^{3+} ions were able to completely quench it at a solution

concentration of 120× 10^{-6} M, followed by Cu^{2+} ions, able to quench the fluorescence almost entirely at a solution concentration of 600 × 10^{-6} M.

✓ The mechanisms under which fluorescence quenching occurred upon addition of metal ions were investigated and the dynamic nature of the mechanism was observed in the case of Fe^{3+}, Mn^{2+}, Cd^{2+} and Ca^{2+} ions and the dynamic-static nature of the other ions (for Fe^{2+} and Pb^{2+} ions the dynamic stage being predominant, and for the rest of the ions the static stage being predominant).

✓ The selectivity studies revealed the affinity of the P-OP-CN compound for Fe^{3+} ions. New solutions of the P-OP-CN polymer were prepared in which the solutions of two metals were added (the first being a tested metal, and the second being Fe^{3+}). It was observed that, upon addition of the second metal, the fluorescence decreases significantly.

✓ Knowing that the fluorescence changes that occur upon the addition of metal ions are caused due to interactions established between the polymer and the metal ions, which involve the formation of chemical complexes, the stoichiometry and bond strength were investigated. The results revealed a 1:2 stoichiometry between Fe^{3+} and P-OP-CN, with strong interactions between the components.

Hydrogels with multiple crosslinks, based on pullulan (P) derivatives, polyvinyl alcohol (PVA) and 3-aminoboronic acid (3-BA)

✓ Several types of hydrogels with multiple crosslinks based on pullulan and PVA have been developed: hydrogels where the polysaccharide component was pullulan oxidized with the TEMPO/NaClO/NaBr or $NaIO_4$ system and hydrogels whose polysaccharide component was the coupling product between the oxidized products and 3-aminoboronic acid.

✓ The crosslinking of hydrogels based on PVA and pullulan dialdehyde are: hydrogen bonds in the hydrogel formed by PVA and pullulan dialdehyde and hydrogen bonds, imine bonds and boronic ester bonds for the hydrogel composed of PVA and pullulan dialdehyde coupled with the boronic acid derivative.

✓ The crosslinking of hydrogels based on PVA and 6-carboxypullulan are: hydrogen bonds and carboxylic ester bonds for the hydrogel composed of PVA and 6-carboxypullulan and hydrogen bonds, amide bonds and boronic ester bonds for the hydrogel composed of PVA and 6-carboxypullulan coupled with boronic acid.

✓ The synthesized hydrogels were analyzed to investigate the porosity and liquid absorption properties. These hydrogels are porous materials, with pores of considerable size, on the order of micrometers. Regarding the swelling capacity, the inclusion of boronic acid leads to a strong absorption which is followed by the material collapse, which indicates a better stability in the dry state than in the wet state of the hydrogels containing boronic acid sequences.

✓ Future experiments involving these hydrogels require to perform new chemical reactions in order to introduce photopolymerizable sequences, capable of forming photocrosslinks through exposure to various radiation sources.

SELECTED BIBLIOGRAPHY

* Mohammed ASA, Naveed M, Jost N. Polysaccharides; classification, chemical properties, and future perspective applications in fields of pharmacology and biological medicine (A review of current applications and upcoming potentialities). Journal of Polymers and the Environment, 29, 2359–2371, 2021.

* Coseri S, Biliuta G,Simionescu BC, Stana-Kleinschek K, Ribitsch V, Harabagiu V. Oxidized cellulose-survey of the most recent achievements. Carbohydrate Polymers, 93, 207215, 2013.

* Adeleye OA, Bamiro OA, Albalawi DA, Alotaibi AS, Iqbal H, Sanyaolu S, Femi-Oyewo MN, Sodeinde KO, Yahaya ZS, Thiripuranathar G, Menaa F. Characterizations of alpha-cellulose and microcrystalline cellulose isolated from cocoa pod husk as a potential pharmaceutical excipient. Materials, 15, 5992, 2022.

* Culica ME, Chibac-Scutaru AL, Asandulesa M, Melinte V, Cojocaru C, Coseri S. Convertible cellulosic platforms with manageable loads of 1-hydroxybenzotriazole: their preparation and conductive behavior. Cellulose, 29, 9847–9863, 2022.

* Raychaudhuri R, Naik S, Shreya AB, Kandpal N, Pandey A, Kalthur G, Mutalik S. Pullulan based stimuli responsive and sub cellular targeted nanoplatforms for biomedical application: synthesis, nanoformulations and toxicological perspective. International Journal of Biological Macromolecules, 161, 1189–1205, 2020.

* Orelma H, Vuoriluoto M, Johansson L-S, Campbell JM, Filpponen I, Biesalski M, Rojas OJ. Preparation of photoreactive nanocellulosic materials via benzophenone grafting. RSC Advances, 6, 85100–85106, 2016.

* Sood A, Gupta A, Agrawal G. Recent advances in polysaccharides based biomaterials for

drug delivery and tissue engineering applications. Carbohydrate Polymer Technologies and Applications, 2, 100067, 2021.

* Singh SR, Kaur N, Singh D, Purewal SS, Kennedy JF. Pullulan in pharmaceutical and cosmeceutical formulations: a review. International Journal of Biological Macromolecules, 231, 123353, 2023.

* Li Z, Lin Z. Recent advances in polysaccharide-based hydrogels for synthesis and applications. Aggregate, 2, 1–26, 2021.

* Chen Y, Li J, Lu J, Ding M, Chen Y. Synthesis and properties of poly(vinyl alcohol) hydrogels with high strength and toughness. Polymer Testing, 108, 107516, 2022.

* Amoresi RAC, Oliveira RC, Marana NL, De Almeida PB, Prata PS, Zaghete MA, Longo E, Sambrano JR, Simões AZ. CeO_2 nanoparticle morphologies and their corresponding crystalline planes for the photocatalytic degradation of organic pollutants. ACS Applied Nano Materials, 2, 6513–6526, 2019.

* Kusmierek E. A CeO2 semiconductor as a photocatalytic and photoelectrocatalytic material for the remediation of pollutants in industrial wastewater: a review. Catalysts, 10, 1435, 2020.

* Dogan-Guner EM, Schueneman GT, Shofner ML, Meredith JC. Acryloyl-modified cellulose nanocrystals: Effects of substitution on crystallinity and copolymerization with acrylic monomers. Cellulose, 28, 10875–10889, 2021.

* Chibac-Scutaru AL, Podasca V, Timpu D, Melinte V. Comparative study on the influence of noble metal nanoparticles (Ag, Au, Pd) on the photocatalytic activity of ZnO NPs embedded in renewable castor oil polymer matrices. Materials, 13, 3468, 2020.

* Ribas-Massonis A,Cicujano M,Duran J,Besalú E,Poater A.Free-radical photopolymerization for curing products for refinish coatings market. Polymers, 14, 2856, 2022.

* Saravanan A, Kumar PS, Jeevanantham S, Karishma S, Tajsabreen B, Yaashikaa PR, Reshma B. Effective water/wastewater treatment methodologies for toxic pollutants removal: processes and applications towards sustainable development. Chemosphere,280,130595, 2021.

* Xu H, Hao Z, Feng W, Wang T, Li Y. Mechanism of photodegradation of organic pollutants in seawater by TiO_2-based photocatalysts and improvement in their performance. ACS Omega, 6, 30698–30707, 2021.

* Gao F, Jiao C, Yu B, Cong H, Shen Y. Preparation and biomedical application of injectable hydrogels. Materials Chemistry Frontiers, 5, 4912–4936, 2021.

* Mo C, Xiang L, Chen Y. Advances in injectable and self-healing polysaccharide hydrogel based on the Schiff base reaction. Macromolecular Rapid Communications,42,2100025, 2021.
* Murariu M, Stroea L. Increasing detection sensitivity of fluorescent polymeric sensors containing fluorescein derivatives by Au NPs. Spectrochimica Acta - Part A: Molecular and Biomolecular Spectroscopy, 291, 122279, 2023.
* Iqhrammullah M, Marlina M, Khalil HPSA, Kurniawan KH, Suyanto H, Hedwig R, Karnadi I, Olaiya NG, Abdullah CK, Abdulmadjid SN. Characterization and performance evaluation of cellulose acetate-polyurethane film for lead II ion removal. Polymers, 12, 1317, 2020.
* Bercea M, Biliuta G, Avadanei M, Baron RI, Butnaru M, Coseri S. Self-healing hydrogels of oxidized pullulan and poly (vinyl alcohol). Carbohydrate Polymers, 206, 210–219, 2019.

ANNEX I – DISSEMINATION OF RESULTS

Works published in ISI-listed scientific journals, the results of which represent the subject of the doctoral thesis:

1. V. Melinte, **Sabina I. Trifan**, A.L. Chibac-Scutaru, V. Podasca, S. Coseri, Reusable catalysts based on CeO_2/cellulose derivative with visible light photocatalytic activity tuned by noble metal nanoparticles inclusion. *Int. J. Biol. Macromol*. 2022, 222, 736-749. **(FI=8.2)**

2. Ioana-Sabina Trifan, A.L. Chibac-Scutaru, V. Melinte, S. Coseri, Photopolymerization Pattern of New Methacrylate Cellulose Acetate Derivatives, *Polymers*,2024, 16, 560. **(FI=4.9)**

3. Ioana-Sabina Trifan, M. Murariu, G. Biliuta, S. Coseri, Two-Step Synthesis of a Pullulan-Derived Polymeric Fluorophore with Metal Ion Sensing Abilities, *Macromol. Rapid Commun.*, 2025, 46, 2400923. **(FI=4.3)**

Works published in ISI-listed scientific journals, the results of which do not constitute the subject of the doctoral thesis:

1. Sabina Ioana Trifan, D. Ivanov, Strategies of hyaluronan chemical modifications for biomedical applications, *Rev. Roum. Chim.*, 2023, 68(5-6), 203-209. **(FI=0.4)**

2. R. Rotaru, V. Melinte, **Ioana-Sabina Trifan***, Biophysical Stimulation for Bone Regeneration with chitosan/barium titanate ferroelectric composite, *P.C.C.P.*, 2024, 26, 13875-13883. **(FI=2.9)**

Works published in non-ISI listed scientific journals:

1. V. Allegra, I. Duceac, **Sabina Trifan**, A. Catini, E. Carino, R. Capuano, K. Pushparaj, C. Di Natale, Organic Electrochemical Transistor as a VOCs Sensor, *Lecture Notes in Electrical Engineering*, 2025, 1134, 94–101.

Oral communications at national and international scientific conferences or mobilities:

1. Ioana-Sabina Trifan, V. Melinte, A.L. Chibac-Scutaru, S. Coseri, Effect of functionalization degree of cellulose derivatives on their properties and photopolymerization profile, *XXXVI Edition of National Chemistry Conference*, "CNChim", Călimănești-Căciulata, Vâlcea, Romania, 4-8th October, **2022**.

2. Ioana-Sabina Trifan, V. Melinte, A.L. Chibac-Scutaru, S. Coseri, Photopolymerization profile of modified cellulose, *3rd Edition of Open Door to The Future. Scientific Communications of Young Researchers*, MacroYouth, Petru Poni Institute of Macromolecular Chemistry, Iasi, 18th November, **2022**.

3. Ioana-Sabina Trifan, Photopolymerization profile of modified cellulose, mobility seminar at Tor Vergata University, Faculty of Chemistry, Rome, Italy, 2nd May, **2023**.

4. Ioana-Sabina Trifan, I.A. Duceac, The experience of an internship at the "Tor Vergata" University in Rome through the Volatevs project, *Final Conference of BioNanoTech-Suport, Support center for Horizon 2020 projects*, Palas, Iasi, Romania, 8th June, **2023**.

5. Ioana-Sabina Trifan, S. Coseri, Flexible network formation by pullulan functionalization with versatile chromophores, *Materials, Methods & Technologies, 25th International Conference*, Burgas, Bulgaria, 17-20th August, **2023**.

6. Ioana-Sabina Trifan, S. Coseri, Increasing the chemical functionality of biopolymers using benzyl amines derivatives - the case of pullulan, *29th Edition of Conference of Progress in Organic and Macromolecular Compounds*, MacroIasi, Petru Poni Institute of Macromolecular Chemistry, Iasi, Romania, 4-6th Octombrie, **2023**.

7. Ioana-Sabina Trifan, M. Murariu, G. Biliuta, S. Coseri, Synthesis, characterization and fluorescent behavior of a chemosensor based on a derivative of pullulan and benzonitrile, *5thEdition of Open Door to the Future Scientific Communications of Young Researchers*, "MacroYouth 2024", 15th November, **2024**, Iasi, Romania. – **Sorin I. Roșca Award of the Romanian Chemical Society**.

8. Ioana-Sabina Trifan, M. Murariu, G. Biliuta, S. Coseri, Investigation of the fluorescent behavior of a pullulan derivative with pending nitrile groups in the presence and the absence of metal ions solution, *8th International Conference of the Doctoral School*, "CSD 2025", 14-16th May, **2025**, "Gheorghe Asachi" University, Iasi, Romania.

9. Ioana-Sabina Trifan, M. Murariu, G. Biliuta, S. Coseri, Fluorescent pullulan derivative with high sensing toward trivalent iron ions detection in wastewaters, *19thInternational Conference on Chemistry and the Environment*, "ICCE 2025", 8-12th June, **2025**, Belgrad,Serbia.

Posters presented at national and international scientific conferences:

1. V. Allegra, I. Duceac, **Sabina Trifan**, A. Catini, F. Caroleo, E. Carino, R. Capuano, K. Pushparaj, C. Di Natale, *Organic Electrochemical Transistor as VOCs Sensors*, XXIIConferenza Nazionale Sensori e Microsistemi, Bologna, Sede Universitaria del Navile, Italy, 7-9th February, 2024.

2. S. Coseri, **S. Trifan**, G. Biliuta, The architectural design and construction of cellulose-based structures for environmental remediation, *19thInternational Conference on Chemistry and the Environment*, "ICCE 2025", 8-12th June, **2025**, Belgrad, Serbia.

Member of working teams for scientific research projects:

1. Research assistant within the project "Photosensitized hybrid coatings based on polyurethane matrices and metal oxide nanoparticles with adjustable photocatalytic characteristics", **PN-III-P4-PCE-2021-0933**.

2. Research assistant within the project "Triple-storey hydrogel powered by multidynamic networks equipped with motion detection abilities", **PN-IV-P1-PCE2023-0558**.

3. Research assistant within the project " Nanocellulosic hybrid Janus aerogels with high floatability for synchronous photocatalytic dyes mineralization and hydrogen production", **PN-IV-P1-PCE-2023-1020**.

Mobilities carried out during the doctoral internship:

1. Faculty of Engineering, Tor Vergata University, Rome, Italy, under the supervision of Prof. Corrado di Natale, 24.04.2023-24.05.2023.